

Dark Matter Physics in General NMSSM

Lei Meng^b, Junjie Cao^{a,c,*}, Fei Li^c, and Shenshen Yang^c

^a *School of Physics, Zhengzhou University, Zhengzhou 450000, China*

^b *School of Physics and Electrical Engineering, Anyang Normal University, Anyang 455000, China*

^c *School of Physics, Henan Normal University, Xinxiang 453007, China*

E-mail: mel18@foxmail.com, junjiecao@alumni.itp.ac.cn,
hnuifeili@163.com, yangshenshen@stu.htu.edu.cn

ABSTRACT: In the General Next-to-Minimal Supersymmetric Standard Model (GNMSSM), singlet particles may form a secluded sector of dark matter (DM), in which Singlino-like DM could achieve the observed relic abundance through various channels such as $\tilde{\chi}_1^0 \tilde{\chi}_1^0 \rightarrow h_s h_s, A_s A_s, h_s A_s$, where h_s and A_s represent singlet-dominated CP-even and CP-odd Higgs bosons. We provide analytical formulas for both the spin-independent and spin-dependent cross sections of Singlino DM scattering with nucleons, illustrating their dependence on the model's parameters in a clear manner. We also present analytic expressions for the annihilation cross sections of these three important channels. Based on these preparations, we conducted Bayesian analyses of the GNMSSM and concluded that the theory significantly favored Singlino-dominated DM over Bino-like DM across a much broader range of parameters. The combined results from our numerical analyses and the formulas distinctly highlight crucial aspects of DM physics within the GNMSSM.

*Corresponding author.

Contents

1	Introduction	1
2	Theoretical preliminaries	4
2.1	Higgs sector of GNMSSM	4
2.2	Neutralino sector of GNMSSM	7
2.3	DM physics of GNMSSM	8
2.3.1	DM relic density	9
2.3.2	DM-nucleon scattering	12
3	Numerical results	14
3.1	Research strategy	14
3.2	Global features	18
3.3	Three annihilation channels	23
4	Summary	30

1 Introduction

Although the presence of non-baryonic dark matter (DM) in the cosmos is compelling from the perspective of astrophysics and cosmological observations and constitutes a pivotal constituent of the prevailing standard model of cosmology, its precise nature remains undetermined. Weakly Interacting Massive Particles (WIMPs) are taken as the favored Cold Dark Matter (CDM) candidates in the standard Λ CDM model. These large-mass, stable particles are favored because they can be produced in thermal equilibrium conditions, and as a consequence, the DM relic density measured by the Planck experiment can be naturally predicted, referred to as the ‘WIMP Miracle’ [1–4]. The WIMPs are typically assumed to couple to Standard Model (SM) particles through weak interactions, resulting in spin-independent (SI) and spin-dependent (SD) scattering cross sections with nucleons around 10^{-45} and 10^{-39} cm², respectively [5]. This coincidence has spurred extensive direct [6–9], indirect [10–12], and collider searches for WIMPs [13, 14]. In particular, recent direct detection experiments like LUX-ZEPLIN (LZ) have achieved unprecedented precision in probing both SI and SD DM-nucleon scatterings but found no evidence of DM, restricting the scattering cross sections to be less than the order of 10^{-47} and 10^{-42} cm², respectively [9]. This implies that the interaction between DM and nucleons is at most feeble, posing significant experimental challenges to simple WIMP theories [15].

Consequently, there is growing interest in exploring scenarios that go beyond the traditional thermal WIMP paradigm.

WIMPs can naturally arise in the supersymmetric extension of the SM in particle physics. Furthermore, supersymmetric theories possess numerous intriguing features, such as the absence of quadratic divergences, gauge coupling unification, and distinctive signatures of supersymmetric particles produced in present and future colliders. In the framework of the Minimal Supersymmetric Standard Model (MSSM), recognized as one of the most economical supersymmetric theories, the neutral electroweakino sector encompasses the mixing of Bino (denoted as \tilde{B}), Wino (referred to as \tilde{W}), and neutral Higgsinos (designated as \tilde{H}_u and \tilde{H}_d), giving rise to the formation of four distinct neutralinos [16–18]. Among these, the lightest mass eigenstate, denoted as $\tilde{\chi}_1^0$, usually corresponds to the lightest supersymmetric particle (LSP) and acts as a feasible candidate of DM. It prefers to be \tilde{B} -dominated and co-annihilate with the \tilde{W} -like electroweakinos to achieve the measured relic abundance. As indicated by the research in Ref. [19], the LZ experiment alone imposes a lower bound on the Higgsino mass, $\mu \gtrsim 380$ GeV, in the absence of strong cancellations between different contributions to the SI scattering. This bound can be enhanced by several tens of GeV after incorporating the radiative correction to the scattering [20, 21]. Although such a large μ may be naturally generated by the well-known Giudice–Masiero mechanism in the gravity-mediated supersymmetry breaking scenario [22], it leads to severe fine-tuning problems in precisely predicting the mass of the Z boson, after considering the Large Hadron Collider (LHC) Higgs discovery and non-observations of any DM and supersymmetric particle signals in experiments when the theory runs down from an ultraviolet high-energy scale to the electroweak scale [23–25].

The dilemma faced by the MSSM inspired us to extend this model. The Next-to-Minimal Supersymmetric Standard Model with a \mathbb{Z}_3 symmetry (\mathbb{Z}_3 -NMSSM) introduces a gauge singlet superfield \hat{S} on top of the MSSM [26, 27]. In this framework, the μ -parameter of the MSSM is dynamically generated once the scalar component of the superfield \hat{S} acquires a vacuum expectation value (vev) below approximately 1 TeV. This places it naturally at the electroweak scale. The neutralino sector includes an additional fermionic partner of \hat{S} , known as the Singlino. Both the Bino-dominated (which is the case in most physical scenarios) and Singlino-dominated neutralinos are viable DM candidates [5, 15, 28–46]. Primarily, the Bino-dominated DM candidate differs from the MSSM given the former’s ability to co-annihilate with a Singlino-dominated neutralino in achieving the measured abundance. Nonetheless, this scenario is confined to an exceedingly limited parameter space defined by specific conditions: $|2\kappa\mu/\lambda| \simeq |M_1|$, moderately large λ and κ , and μ values exceeding 300 GeV [5, 15]. This space predicts a significant mixing of the SM Higgs field with the singlet Higgs field and is thus disfavored by the Higgs property measurements at the LHC. The characteristics of Singlino-dominated DM are contingent upon the

values of λ , $\tan\beta$, $m_{\tilde{\chi}_1^0}$, and $\mu_{\text{eff}} \equiv \lambda v_s/\sqrt{2}$ [47], where λ denotes the singlet–doublet Higgs Yukawa coupling within the superpotential and $m_{\tilde{\chi}_1^0} \simeq 2\kappa\mu/\lambda$ requires $2|\kappa|/\lambda < 1$. Considering that both SI and SD DM-nucleon scattering cross sections scale with λ^4 in the regime of heavy singlet Higgs bosons and consequently, the LZ experiment generally sets an upper limit of $\lambda \lesssim 0.1$, the DM is likely to achieve the observed abundance through one of two main mechanisms [31]: co-annihilating with Higgsino-dominated electroweakinos or undergoing resonant annihilations facilitated by singlet-dominated CP-even or CP-odd Higgs bosons. The former scenario is only viable within a narrow parameter space characterized by $2|\kappa|/\lambda \simeq 1$, $\lambda < 0.1$, and $\mu < 400$ GeV, where κ represents the self-coupling coefficient of the singlet Higgs field [47]. To achieve the measured density, the latter scenario requires $2|m_{\tilde{\chi}_1^0}|$ to be close to the scalar mass. Thus, all these scenarios correspond to an exceptionally constrained parameter space, resulting in a significant suppression of Bayesian evidence¹.

The situation becomes different in the General NMSSM (GNMSSM), where both λ and κ can play distinct roles in DM physics [49, 50]. Specifically, the relationship that holds for Singlino DM in the \mathbb{Z}_3 -NMSSM, i.e., $2|\kappa|/\lambda < 1$, no longer applies, implying that $|\kappa|$ can be significantly larger than λ . In this case, particles predominantly comprising the singlet sector, including the Singlino-dominated DM and singlet-dominated Higgs bosons, can form an isolated DM sector [51], where the DM attains the correct relic abundance by tuning the value of κ and through processes such as $\tilde{\chi}_1^0 \tilde{\chi}_1^0 \rightarrow h_s A_s, h_s h_s, A_s A_s$. Here, h_s and A_s denote singlet-dominated CP-even and CP-odd Higgs bosons, respectively. Similar to the situation of \mathbb{Z}_3 -NMSSM, the SI DM-nucleon scattering rate is proportional to $\lambda^2 \kappa^2$ for moderately light h_s and λ^4 for very massive h_s . It is thus suppressed to satisfy the LZ restrictions for a small λ . As a result, the vacuum of the scalar potential in the GNMSSM becomes more stable than that of the MSSM [52, 53]. Additionally, given the singlet nature of the DM and the complex mass hierarchy, the decay chains of heavy supersymmetric particles in the GNMSSM are lengthened compared to the prediction of the MSSM, which causes their detection at the LHC to be rather tricky. These characteristics allow a more extensive parameter space of the GNMSSM to be consistent with current experimental results.

¹Bayesian evidence is a fundamental concept in Bayesian statistics [48]. It is typically denoted as $Z(D|M) \equiv \int P(D|O(M, \Theta))P(\Theta|M) \prod d\theta_i$, where $P(\Theta|M)$ represents the prior probability density function of input parameters $\Theta = (\Theta_1, \Theta_2, \dots)$ in model M , and $P(D|O(M, \Theta)) \equiv \mathcal{L}(\Theta)$ is the likelihood function for observed values O . The Bayesian evidence considers both the theoretical predictions $O(M, \Theta)$ and the experimental data D , and its computation involves marginalizing the model’s parameters, which requires integrating the likelihood function and prior probability over all possible parameter values. In Bayesian statistics, evidence is used to compare different models and determine which one is more plausible for explaining the observed data. While a higher value of Z suggests that the respective model is more likely to agree with the data, an extremely small Z means that the theory requires its parameters to be fine-tuned for the same.

Based on the challenges faced by the MSSM and \mathbb{Z}_3 -NMSSM, an extensive investigation of the DM physics in the GNMSSM was performed in this study. The rest of this paper is organized as follows. Section 2 outlines the properties of the GNMSSM, Section 3 describes the research strategy and numerical results to elucidate the characteristics of DM physics, and Section 4 provides a summary of the research findings.

2 Theoretical preliminaries

The GNMSSM augments the MSSM by a gauge singlet superfield \hat{S} that does not carry any leptonic or baryonic number. Thus, its Higgs sector contains \hat{S} and two $SU(2)_L$ doublet superfields, $\hat{H}_u = (\hat{H}_u^+, \hat{H}_u^0)$ and $\hat{H}_d = (\hat{H}_d^0, \hat{H}_d^-)$. The general form of its superpotential is given by [26]

$$W_{\text{GNMSSM}} = W_{\text{Yukawa}} + \lambda \hat{S} \hat{H}_u \cdot \hat{H}_d + \frac{\kappa}{3} \hat{S}^3 + \mu \hat{H}_u \cdot \hat{H}_d + \frac{1}{2} \mu' \hat{S}^2 + \xi \hat{S}, \quad (2.1)$$

where W_{Yukawa} is the MSSM superpotential containing quark and lepton Yukawa couplings, and the dimensionless coupling coefficients λ and κ parameterize the interactions between the Higgs fields, the same as those of the \mathbb{Z}_3 -NMSSM. The bilinear mass parameters μ and μ' and the singlet tadpole parameter ξ depict \mathbb{Z}_3 -symmetry-violating effects, which are advantageous for solving the tadpole problem [26, 54] and the cosmological domain-wall problem of the \mathbb{Z}_3 -NMSSM [55–57]. Given that one of these parameters can be eliminated by shifting the \hat{S} field by a particular constant and redefining the other parameters [58], we set ξ to be zero without losing the generality of this study. As suggested by previous studies [55, 58–61], the natural values of the electroweak order for μ and μ' may arise from breaking the fundamental discrete R -symmetry, \mathbb{Z}_4^R or \mathbb{Z}_8^R , at high energy scales. They can significantly change the properties of neutral Higgs bosons and neutralinos and predict richer phenomenology than the \mathbb{Z}_3 -NMSSM, which is the focus of this study.

2.1 Higgs sector of GNMSSM

The soft supersymmetry-breaking Lagrangian for the Higgs fields in the GNMSSM is given by

$$-\mathcal{L}_{\text{soft}} = \left[\lambda A_\lambda S H_u \cdot H_d + \frac{1}{3} \kappa A_\kappa S^3 + m_3^2 H_u \cdot H_d + \frac{1}{2} m_S'^2 S^2 + \xi' S + h.c. \right] + m_{H_u}^2 |H_u|^2 + m_{H_d}^2 |H_d|^2 + m_S^2 |S|^2, \quad (2.2)$$

where H_u , H_d , and S denote the scalar components of the Higgs superfields, and $m_{H_u}^2$, $m_{H_d}^2$, and m_S^2 are their supersymmetry-breaking masses. After the electroweak symmetry breaking, the neutral Higgs fields acquire non-zero vevs:

$$\langle H_u^0 \rangle = v_u / \sqrt{2}, \quad \langle H_d^0 \rangle = v_d / \sqrt{2}, \quad \langle S \rangle = v_s / \sqrt{2}, \quad (2.3)$$

with $v = \sqrt{v_u^2 + v_d^2} \simeq 246$ GeV, and the three masses are determined in solving the conditional equations to minimize the scalar potential. The Higgs sector is then described by eleven free parameters:

$$\tan \beta, \lambda, \kappa, v_s, A_\lambda, A_\kappa, \mu, \mu', m_3^2, m_S'^2, \xi', \quad (2.4)$$

where $\tan \beta$ is defined by $\tan \beta \equiv v_u/v_d$.

In revealing the properties of Higgs physics, it is customary to work with the field combinations of $H_{\text{SM}} \equiv \sin \beta \text{Re}(H_u^0) + \cos \beta \text{Re}(H_d^0)$, $H_{\text{NSM}} \equiv \cos \beta \text{Re}(H_u^0) - \sin \beta \text{Re}(H_d^0)$, and $A_{\text{NSM}} \equiv \cos \beta \text{Im}(H_u^0) - \sin \beta \text{Im}(H_d^0)$, where H_{SM} denotes the SM Higgs field, and H_{NSM} and A_{NSM} represent the extra doublet Higgs fields [62, 63]. In the bases $(H_{\text{NSM}}, H_{\text{SM}}, \text{Re}[S])$, the mass matrix of the CP-even Higgs fields takes the following form [26, 63]

$$\begin{aligned} \mathcal{M}_{S,11}^2 &= \frac{\lambda v_s(\sqrt{2}A_\lambda + \kappa v_s + \sqrt{2}\mu') + 2m_3^2}{\sin 2\beta} + \frac{1}{2}(2m_Z^2 - \lambda^2 v^2) \sin^2 2\beta, \\ \mathcal{M}_{S,12}^2 &= -\frac{1}{4}(2m_Z^2 - \lambda^2 v^2) \sin 4\beta, \quad \mathcal{M}_{S,13}^2 = -\frac{\lambda v}{\sqrt{2}}(A_\lambda + \sqrt{2}\kappa v_s + \mu') \cos 2\beta, \\ \mathcal{M}_{S,22}^2 &= m_Z^2 \cos^2 2\beta + \frac{1}{2}\lambda^2 v^2 \sin^2 2\beta, \\ \mathcal{M}_{S,23}^2 &= \frac{\lambda v}{\sqrt{2}} \left[(\sqrt{2}\lambda v_s + 2\mu) - (A_\lambda + \sqrt{2}\kappa v_s + \mu') \sin 2\beta \right], \\ \mathcal{M}_{S,33}^2 &= \frac{(A_\lambda + \mu') \sin 2\beta}{2\sqrt{2}v_s} \lambda v^2 + \frac{\kappa v_s}{\sqrt{2}}(A_\kappa + 2\sqrt{2}\kappa v_s + 3\mu') - \frac{\mu}{\sqrt{2}v_s} \lambda v^2 - \frac{\sqrt{2}}{v_s} \xi'. \end{aligned} \quad (2.5)$$

In the bases $(A_{\text{NSM}}, \text{Im}(S))$, the elements of the CP-odd Higgs matrix are given by

$$\begin{aligned} \mathcal{M}_{P,11}^2 &= \frac{\lambda v_s(\sqrt{2}A_\lambda + \kappa v_s + \sqrt{2}\mu') + 2m_3^2}{\sin 2\beta}, \quad \mathcal{M}_{P,12}^2 = \frac{\lambda v}{\sqrt{2}}(A_\lambda - \sqrt{2}\kappa v_s - \mu'), \\ \mathcal{M}_{P,22}^2 &= \frac{(A_\lambda + 2\sqrt{2}\kappa v_s + \mu') \sin 2\beta}{2\sqrt{2}v_s} \lambda v^2 - \frac{\kappa v_s}{\sqrt{2}}(3A_\kappa + \mu') \\ &\quad - \frac{\mu}{\sqrt{2}v_s} \lambda v^2 - 2m_S'^2 - \frac{\sqrt{2}}{v_s} \xi'. \end{aligned} \quad (2.6)$$

Three CP-even mass eigenstates $h_i = \{h, H, h_s\}$ and two CP-odd mass eigenstates $a_i = \{A_H, A_s\}$ are acquired through unitary rotations of V and V_P to diagonalize \mathcal{M}_S^2 and \mathcal{M}_P^2 , respectively, leading to

$$\begin{aligned} h_i &= V_{h_i}^{\text{NSM}} H_{\text{NSM}} + V_{h_i}^{\text{SM}} H_{\text{SM}} + V_{h_i}^{\text{S}} \text{Re}[S], \\ a_i &= V_{P,a_i}^{\text{NSM}} A_{\text{NSM}} + V_{P,a_i}^{\text{S}} \text{Im}[S]. \end{aligned} \quad (2.7)$$

Among these states, h corresponds to the scalar discovered at the LHC, H and A_H represent heavy doublet-dominated Higgs bosons, and h_s and A_s denote singlet-dominated states. These states are also labeled as h_i ($i=1,2,3$) and A_j ($j=1,2$) in

ascending mass orders for convenience, i.e., $m_{h_1} < m_{h_2} < m_{h_3}$ and $m_{A_1} < m_{A_2}$ in this study. Therefore, $h \equiv h_1$ and $m_{h_s} > m_h$ for the h_1 scenario, and $h \equiv h_2$ and $m_h > m_{h_s}$ for the h_2 scenario. The model also predicts a pair of charged Higgs bosons, $H^\pm = \cos \beta H_u^\pm + \sin \beta H_d^\pm$, with their masses given by

$$m_{H^\pm}^2 = \frac{\lambda v_s (\sqrt{2} A_\lambda + \kappa v_s + \sqrt{2} \mu') + 2m_3^2}{\sin 2\beta} + m_W^2 - \frac{1}{2} \lambda^2 v^2. \quad (2.8)$$

Note that charged Higgs bosons H^\pm degenerate with the CP-even doublet scalar H and the CP-odd scalar A_H in mass.

So far, the LHC experiments have performed intensive searches for the additional Higgs bosons H , A_H , H^\pm , h_s , and A_s and set limits on their properties, such as their masses and couplings [64, 65]. We note that the parameters μ , μ' , m_3^2 , $m_S'^2$, and ξ' are not directly related to experimental measurements. This motivated us to use the masses of CP-odd heavy doublet Higgs field, CP-even and -odd singlet Higgs fields, and Higgsino and Singlino fields, denoted as $m_A \equiv \sqrt{\mathcal{M}_{P,11}^2}$, $m_B \equiv \sqrt{\mathcal{M}_{S,33}^2}$, $m_C \equiv \sqrt{\mathcal{M}_{P,22}^2}$, $\mu_{\text{tot}} \equiv \mu_{\text{eff}} + \mu$, and $m_N \equiv \frac{2\kappa}{\lambda} \mu_{\text{eff}} + \mu'$, respectively, as theoretical inputs. The former set of parameters are then given by

$$\begin{aligned} \mu &= \mu_{\text{tot}} - \frac{\lambda}{\sqrt{2}} v_s, \quad \mu' = m_N - \sqrt{2} \kappa v_s, \quad m_3^2 = \frac{m_A^2 \sin 2\beta}{2} - \lambda v_s \left(\frac{\kappa v_s}{2} + \frac{\mu'}{\sqrt{2}} + \frac{A_\lambda}{\sqrt{2}} \right), \\ \xi' &= \frac{v_s}{\sqrt{2}} \left[\frac{(A_\lambda + \mu') \sin 2\beta}{2\sqrt{2} v_s} \lambda v^2 + \frac{\kappa v_s}{\sqrt{2}} (A_\kappa + 2\sqrt{2} \kappa v_s + 3\mu') - \frac{\mu}{\sqrt{2} v_s} \lambda v^2 - m_B^2 \right], \\ m_S'^2 &= \frac{1}{2} \left[m_B^2 - m_C^2 + \lambda \kappa \sin 2\beta v^2 - 2\sqrt{2} \kappa v_s (A_\kappa + \frac{\kappa}{\sqrt{2}} v_s + \mu') \right], \end{aligned} \quad (2.9)$$

and Eqs. (2.5), (2.6), and (2.8) take the following simplified forms:

$$\begin{aligned} \mathcal{M}_{S,11}^2 &= m_A^2 + \frac{1}{2} (2m_Z^2 - \lambda^2 v^2) \sin^2 2\beta, \quad \mathcal{M}_{S,12}^2 = -\frac{1}{4} (2m_Z^2 - \lambda^2 v^2) \sin 4\beta, \\ \mathcal{M}_{S,13}^2 &= -\frac{\lambda v}{\sqrt{2}} (A_\lambda + m_N) \cos 2\beta, \quad \mathcal{M}_{S,22}^2 = m_Z^2 \cos^2 2\beta + \frac{1}{2} \lambda^2 v^2 \sin^2 2\beta, \\ \mathcal{M}_{S,23}^2 &= \frac{\lambda v}{\sqrt{2}} [2\mu_{\text{tot}} - (A_\lambda + m_N) \sin 2\beta], \quad \mathcal{M}_{S,33}^2 = m_B^2, \quad \mathcal{M}_{P,11}^2 = m_A^2, \\ \mathcal{M}_{P,22}^2 &= m_C^2, \quad \mathcal{M}_{P,12}^2 = \frac{\lambda v}{\sqrt{2}} (A_\lambda - m_N), \quad m_{H^\pm}^2 = m_A^2 + m_W^2 - \frac{1}{2} \lambda^2 v^2. \end{aligned} \quad (2.10)$$

These formulas indicate that the Higgs mass matrices are determined by just eight out of the eleven parameters: $\tan \beta$, λ , A_λ , m_A , m_B , m_C , m_N , and μ_{tot} . As will be shown in Eqs. (2.19-2.21), the remaining three parameters, κ , A_κ , and v_s , specifically influence triple Higgs coupling strengths.

In the case of very massive charged Higgs bosons, the following approximations hold [5]:

$$m_{h_s}^2 \simeq m_B^2 - \frac{\mathcal{M}_{S,13}^4}{m_A^2 - m_B^2}, \quad m_{A_s}^2 \simeq m_C^2 - \frac{\mathcal{M}_{P,12}^4}{m_A^2 - m_C^2}, \quad \frac{V_{P,A_s}^{\text{NSM}}}{V_{P,A_s}^{\text{S}}} = \frac{\mathcal{M}_{P,12}^2}{m_{A_s}^2 - m_A^2} \simeq 0,$$

$$\begin{aligned}
\frac{V_h^S}{V_h^{\text{SM}}} &\simeq \frac{\mathcal{M}_{S,23}^2}{m_h^2 - m_B^2}, & V_h^{\text{NSM}} &\sim 0, & V_h^{\text{SM}} &\simeq \sqrt{1 - \left(\frac{V_h^S}{V_h^{\text{SM}}}\right)^2} \sim 1, \\
\frac{V_{h_s}^{\text{SM}}}{V_{h_s}^S} &\simeq \frac{\mathcal{M}_{S,23}^2}{m_{h_s}^2 - m_h^2}, & V_{h_s}^{\text{NSM}} &\sim 0, & V_{h_s}^S &\simeq \sqrt{1 - \left(\frac{V_{h_s}^{\text{SM}}}{V_{h_s}^S}\right)^2} \sim 1.
\end{aligned} \tag{2.11}$$

Evidently, the singlet fields will decouple from the doublet Higgs fields in the limit of $\lambda \rightarrow 0$, and the field masses m_B , m_C , and m_N can be regarded as physical particle masses to a good approximation. Additionally, the singlet masses are independent and may all take small values since they are weakly constrained by current experiments.

2.2 Neutralino sector of GNMSSM

The mixing between fermionic partners for neutral Higgs bosons and gauginos results in five neutralinos and two charginos, denoted as $\tilde{\chi}_i^0$ ($i = 1, \dots, 5$) and $\tilde{\chi}_i^\pm$ ($i = 1, 2$), respectively. In the gauge eigenstate bases $\psi^0 = (-i\tilde{B}, -i\tilde{W}, \tilde{H}_d^0, \tilde{H}_u^0, \tilde{S})$, the symmetric neutralino mass matrix is given by [26]

$$M_{\tilde{\chi}^0} = \begin{pmatrix} M_1 & 0 & -m_Z \sin \theta_W \cos \beta & m_Z \sin \theta_W \sin \beta & 0 \\ & M_2 & m_Z \cos \theta_W \cos \beta & -m_Z \cos \theta_W \sin \beta & 0 \\ & & 0 & -\mu_{\text{tot}} & -\frac{1}{\sqrt{2}}\lambda v \sin \beta \\ & & & 0 & -\frac{1}{\sqrt{2}}\lambda v \cos \beta \\ & & & & m_N \end{pmatrix}, \tag{2.12}$$

where M_1 and M_2 are gaugino soft-breaking masses, $s_W = \sin \theta_W$, and $c_w = \cos \theta_W$. We use the rotation matrix N to diagonalize this mass matrix and label the resulting mass eigenstates by an ascending mass order

$$\tilde{\chi}_i^0 = N_{i1}\psi_1^0 + N_{i2}\psi_2^0 + N_{i3}\psi_3^0 + N_{i4}\psi_4^0 + N_{i5}\psi_5^0, \tag{2.13}$$

where the matrix elements N_{i3} and N_{i4} characterize the \tilde{H}_d^0 and \tilde{H}_u^0 components in $\tilde{\chi}_i^0$, and N_{i5} denotes the Singlino component. We say $\tilde{\chi}_1^0$ is Singlino-dominated if $N_{15}^2 > 0.5$.

In the case that the gauginos are very massive and $\mu_{\text{tot}}^2 - m_N^2 \gg \lambda^2 v^2$, the following approximations for the Singlino-dominated $m_{\tilde{\chi}_1^0}$ hold [66–68]:

$$\begin{aligned}
m_{\tilde{\chi}_1^0} &\simeq m_N + \frac{1}{2} \frac{\lambda^2 v^2 (m_{\tilde{\chi}_1^0} - \mu_{\text{tot}} \sin 2\beta)}{m_{\tilde{\chi}_1^0}^2 - \mu_{\text{tot}}^2} \simeq m_N, & N_{11} &\sim 0, & N_{12} &\sim 0, \\
\frac{N_{13}}{N_{15}} &= \frac{\lambda v}{\sqrt{2}\mu_{\text{tot}}} \frac{(m_{\tilde{\chi}_1^0}/\mu_{\text{tot}}) \sin \beta - \cos \beta}{1 - (m_{\tilde{\chi}_1^0}/\mu_{\text{tot}})^2}, & \frac{N_{14}}{N_{15}} &= \frac{\lambda v}{\sqrt{2}\mu_{\text{tot}}} \frac{(m_{\tilde{\chi}_1^0}/\mu_{\text{tot}}) \cos \beta - \sin \beta}{1 - (m_{\tilde{\chi}_1^0}/\mu_{\text{tot}})^2}, \\
N_{15}^2 &\simeq \left(1 + \frac{N_{13}^2}{N_{15}^2} + \frac{N_{14}^2}{N_{15}^2}\right)^{-1}
\end{aligned} \tag{2.14}$$

$$= \frac{\left[1 - (m_{\tilde{\chi}_1^0}/\mu_{\text{tot}})^2\right]^2}{\left[(m_{\tilde{\chi}_1^0}/\mu_{\text{tot}})^2 - 2(m_{\tilde{\chi}_1^0}/\mu_{\text{tot}}) \sin 2\beta + 1\right] \left(\frac{\lambda v}{\sqrt{2}\mu_{\text{tot}}}\right)^2 + \left[1 - (m_{\tilde{\chi}_1^0}/\mu_{\text{tot}})^2\right]^2}.$$

The ratio of the Higgsino fraction in $\tilde{\chi}_1^0$, denoted as $Z_h \equiv N_{13}^2 + N_{14}^2$, to the Singlino fractions $Z_s \equiv N_{15}^2$ is acquired by

$$\frac{Z_h}{Z_s} = \left(\frac{\lambda v}{\sqrt{2}\mu_{\text{tot}}}\right)^2 \frac{\left(m_{\tilde{\chi}_1^0}/\mu_{\text{tot}}\right)^2 - 2(m_{\tilde{\chi}_1^0}/\mu_{\text{tot}}) \sin 2\beta + 1}{\left[1 - \left(m_{\tilde{\chi}_1^0}/\mu_{\text{tot}}\right)^2\right]^2}. \quad (2.15)$$

These approximations reveal that the characteristics of $\tilde{\chi}_1^0$ are represented by five independent parameters: $\tan \beta$, λ , κ , μ_{tot} , and $m_{\tilde{\chi}_1^0}$, where κ quantifies the self-interactions of the singlet fields. They reflect that both λ and μ_{tot} play a significant role in determining Z_h ; specifically, a smaller λ or a larger μ_{tot} can suppress Z_h . Notably, if one chooses m_N , or equivalently $m_{\tilde{\chi}_1^0}$, as a theoretical input, κ does not explicitly affect $m_{\tilde{\chi}_1^0}$, and it is independent of λ in influencing the other properties of $\tilde{\chi}_1^0$. This feature distinguishes it from the Singlino-dominated $\tilde{\chi}_1^0$ in the Z_3 -NMSSM, whose properties are determined by four parameters, i.e., $\tan \beta$, λ , μ_{eff} , and $m_{\tilde{\chi}_1^0} \simeq 2\kappa\mu_{\text{eff}}/\lambda$, with κ satisfying $2|\kappa| < \lambda$ [47].

We point out the difference between the GNMSSM and μ -extended NMSSM discussed in Ref. [49]: in the former, the singlet masses m_B , m_C , and m_N and the Higgsino mass μ_{tot} are independent, while in the latter, they are correlated.

2.3 DM physics of GNMSSM

In the GNMSSM, the following interactions are pertinent to the DM physics [26]:

$$\begin{aligned} C_{\tilde{\chi}_1^0 \tilde{\chi}_1^0 h_i} &= V_{h_i}^{\text{SM}} C_{\tilde{\chi}_1^0 \tilde{\chi}_1^0 H_{\text{SM}}} + V_{h_i}^{\text{NSM}} C_{\tilde{\chi}_1^0 \tilde{\chi}_1^0 H_{\text{NSM}}} + V_{h_i}^{\text{S}} C_{\tilde{\chi}_1^0 \tilde{\chi}_1^0 \text{Re}[S]} \\ &\simeq \sqrt{2}\lambda \left[V_{h_i}^{\text{SM}} N_{15} (N_{13} \sin \beta + N_{14} \cos \beta) + V_{h_i}^{\text{NSM}} N_{15} (N_{13} \cos \beta - N_{14} \sin \beta) \right] \\ &\quad + \sqrt{2}V_{h_i}^{\text{S}} (\lambda N_{13} N_{14} - \kappa N_{15}^2), \end{aligned} \quad (2.16)$$

$$\begin{aligned} C_{\tilde{\chi}_1^0 \tilde{\chi}_1^0 a_i} &= V_{P,a_i}^{\text{NSM}} C_{\tilde{\chi}_1^0 \tilde{\chi}_1^0 A_{\text{NSM}}} + V_{P,a_i}^{\text{S}} C_{\tilde{\chi}_1^0 \tilde{\chi}_1^0 \text{Im}[S]} \\ &\simeq -\sqrt{2}V_{P,a_i}^{\text{NSM}} \lambda N_{15} (N_{13} \cos \beta + N_{14} \sin \beta) + \sqrt{2}V_{P,a_i}^{\text{S}} (\lambda N_{13} N_{14} - \kappa N_{15}^2), \end{aligned} \quad (2.17)$$

$$C_{\tilde{\chi}_1^0 \tilde{\chi}_1^0 Z} = \frac{m_Z}{v} (N_{13}^2 - N_{14}^2), \quad C_{\tilde{\chi}_1^0 \tilde{\chi}_1^0 G^0} \simeq -\sqrt{2}\lambda N_{15} (N_{13} \sin \beta - N_{14} \cos \beta), \quad (2.18)$$

$$\begin{aligned} C_{h_i h_s h_s} &= \lambda v V_{h_i}^{\text{SM}} V_{h_s}^{\text{S}} V_{h_s}^{\text{S}} (\lambda - \kappa \sin 2\beta) - \lambda \kappa v V_{h_i}^{\text{NSM}} V_{h_s}^{\text{S}} V_{h_s}^{\text{S}} \cos 2\beta \\ &\quad + \sqrt{2}\kappa V_{h_i}^{\text{S}} V_{h_s}^{\text{S}} V_{h_s}^{\text{S}} (3m_N + A_\kappa) + C'_{h_s}(\lambda, \kappa, \tan \beta, v_s, A_\lambda, m_N), \end{aligned} \quad (2.19)$$

$$\begin{aligned} C_{h_i A_s A_s} &= \lambda v V_{h_i}^{\text{SM}} (\lambda + \kappa \sin 2\beta) + \lambda \kappa v V_{h_i}^{\text{NSM}} \cos 2\beta \\ &\quad + \sqrt{2}\kappa V_{h_i}^{\text{S}} (m_N - A_\kappa) + C'_{A_s}(\lambda, \kappa, \tan \beta, v_s, A_\lambda, m_N), \end{aligned} \quad (2.20)$$

where the last contributions in $C_{h_i h_s h_s}$ and $C_{h_i A_s A_s}$ are suppressed by the Higgs mixings and they are functions of λ , κ , $\tan \beta$, v_s , A_λ , and m_N . In the small λ case,

we conclude that

$$\begin{aligned} C_{\tilde{\chi}_1^0 \tilde{\chi}_1^0 h_s} &\simeq C_{\tilde{\chi}_1^0 \tilde{\chi}_1^0 A_s} \simeq -\sqrt{2}\kappa, & C_{h_s h_s h_s} &\simeq \sqrt{2}\kappa(3m_N + A_\kappa), \\ C_{h_s A_s A_s} &\simeq \sqrt{2}\kappa(m_N - A_\kappa), \end{aligned} \quad (2.21)$$

and the other interactions, such as $C_{\tilde{\chi}_1^0 \tilde{\chi}_1^0 h}$, $C_{\tilde{\chi}_1^0 \tilde{\chi}_1^0 Z}$, $C_{hh_s h_s}$, and $C_{h A_s A_s}$, are suppressed by λ . These characteristics are crucial to understand the results of this study.

2.3.1 DM relic density

The thermally averaged cross section for WIMP DM pair annihilation under a non-relativistic approximation and in the absence of co-annihilation can be expanded as [3, 69]

$$\langle \sigma_A v \rangle = a + b \langle v^2 \rangle + \mathcal{O}(\langle v^4 \rangle) \approx a + 6 \frac{b}{x}, \quad (2.22)$$

where a corresponds to the s -wave contribution at a zero relative velocity, b encompasses contributions from both s -wave and p -wave processes, and $x \equiv m_{\tilde{\chi}_1^0}/T$, with T denoting the temperature of the early Universe. After integrating the density function from the freeze-out temperature $x_F = m/T_F$ to infinity, the present thermal relic abundance is given by [5]

$$\Omega h^2 = 0.12 \left(\frac{80}{g_*} \right)^{1/2} \left(\frac{x_F}{25} \right) \left(\frac{2.3 \times 10^{-26} \text{cm}^3/\text{s}}{\langle \sigma v \rangle_{x_F}} \right), \quad (2.23)$$

where $g_* \sim 80$ is the total number of effectively relativistic degrees of freedom at the time of freeze-out, and $x_F \sim 25$ is obtained by solving the freeze-out equation in [69].

As indicated by the following study, the GNMSSM predicts a Singlino-dominated DM in most cases and achieves the observed relic abundance primarily through the following channels:

1. $\tilde{\chi}_1^0 \tilde{\chi}_1^0 \rightarrow h_s h_s$

This channel, which can be the most important annihilation of $\tilde{\chi}_1^0$ when $m_{\tilde{\chi}_1^0} > m_{h_s}$ and $m_{A_s} > 2m_{\tilde{\chi}_1^0} - m_{h_s}$, occurs by the s -channel exchange of CP-even Higgs bosons and t -channel exchange of neutralinos. The full analytic expression of $\langle \sigma v \rangle_{x_F}^{h_s h_s}$ is very complex [70]. However, this can be significantly simplified in the case of minor λ paired with significant $|\kappa|$, where only the contributions from the exchanges of h_s and $\tilde{\chi}_1^0$ are crucial. Correspondingly, $\langle \sigma v \rangle_{x_F}^{h_s h_s}$ is approximated by [71]

$$\begin{aligned} \langle \sigma v \rangle_{x_F}^{h_s h_s} &\simeq \frac{v_F^2}{192\pi m_{\tilde{\chi}_1^0}^2} \sqrt{1 - \frac{m_{h_s}^2}{m_{\tilde{\chi}_1^0}^2}} \times \left\{ \frac{8C_{h_s h_s h_s} C_{\tilde{\chi}_1^0 \tilde{\chi}_1^0 h_s}^3 m_{\tilde{\chi}_1^0}^3 (2m_{h_s}^2 - 5m_{\tilde{\chi}_1^0}^2)}{(m_{h_s}^2 - 4m_{\tilde{\chi}_1^0}^2)(m_{h_s}^2 - 2m_{\tilde{\chi}_1^0}^2)} \right. \\ &\quad \left. + \frac{3C_{h_s h_s h_s}^2 C_{\tilde{\chi}_1^0 \tilde{\chi}_1^0 h_s}^2 m_{\tilde{\chi}_1^0}^2}{(m_{h_s}^2 - 4m_{\tilde{\chi}_1^0}^2)^2} + \frac{16C_{\tilde{\chi}_1^0 \tilde{\chi}_1^0 h_s}^4 (9m_{\tilde{\chi}_1^0}^8 - 8m_{\tilde{\chi}_1^0}^6 m_{h_s}^2 + 2m_{h_s}^8)}{(m_{h_s}^2 - 2m_{\tilde{\chi}_1^0}^2)^4} \right\}. \end{aligned} \quad (2.24)$$

This formula together with Eq. (2.21) indicate that $\langle\sigma v\rangle_{x_F}^{h_s h_s}$ depends mainly on κ , A_κ , m_{h_s} , and $m_{\tilde{\chi}_1^0}$. In particular, κ plays a critical role in determining the magnitude of $\langle\sigma v\rangle_{x_F}^{h_s h_s}$, since most of its dominant contributions are proportional to κ^4 . If $C_{h_s h_s h_s}$ is sufficiently small so that the s-channel contribution can be neglected, we have

$$\langle\sigma v\rangle_{x_F}^{h_s h_s} \simeq \frac{3v_F^2 \kappa^4}{16\pi m_{\tilde{\chi}_1^0}^2}, \quad (2.25)$$

if $m_{\tilde{\chi}_1^0}^2 \gg m_{h_s}^2$, which implies that

$$|\kappa| \sim 0.23 \times \left(\frac{m_{\tilde{\chi}_1^0}}{300 \text{ GeV}} \right)^{1/2}, \quad (2.26)$$

allowing the observed density to be acquired.

2. $\tilde{\chi}_1^0 \tilde{\chi}_1^0 \rightarrow A_s A_s$

This channel can be the dominant annihilation of $\tilde{\chi}_1^0$ if $m_{\tilde{\chi}_1^0} > m_{A_s}$ and $m_{h_s} > 2m_{\tilde{\chi}_1^0} - m_{A_s}$. It proceeds in a way similar to $\tilde{\chi}_1^0 \tilde{\chi}_1^0 \rightarrow h_s h_s$, and $\langle\sigma v\rangle_{x_F}^{A_s A_s}$ is given by [71]

$$\langle\sigma v\rangle_{x_F}^{A_s A_s} \simeq \frac{v_F^2}{128\pi m_{\tilde{\chi}_1^0}^2} \sqrt{1 - \frac{m_{A_s}^2}{m_{\tilde{\chi}_1^0}^2}} \times \left\{ \frac{32}{3} \frac{C_{\tilde{\chi}_1^0 \tilde{\chi}_1^0 A_s}^4 m_{\tilde{\chi}_1^0}^4 (m_{A_s}^2 - m_{\tilde{\chi}_1^0}^2)^2}{(m_{A_s}^2 - 2m_{\tilde{\chi}_1^0}^2)^4} + \frac{4C_{\tilde{\chi}_1^0 \tilde{\chi}_1^0 h_s}^2 C_{\tilde{\chi}_1^0 \tilde{\chi}_1^0 A_s}^2 m_{\tilde{\chi}_1^0}^2 m_{h_s}^2}{(m_{h_s}^2 - 4m_{\tilde{\chi}_1^0}^2)^2 + m_{h_s}^2 \Gamma_{h_s}^2} \right\}. \quad (2.27)$$

Compared with $\langle\sigma v\rangle_{x_F}^{h_s h_s}$, $\langle\sigma v\rangle_{x_F}^{A_s A_s}$ relies on one more parameter, m_{A_s} , and for $m_{h_s} \simeq 2m_{\tilde{\chi}_1^0}$, it can be resonantly enhanced. As a result, it possesses more complex features than $\langle\sigma v\rangle_{x_F}^{h_s h_s}$. Similar to the previous discussion, if we neglect the s-channel contribution and assume $m_{\tilde{\chi}_1^0}^2 \gg m_{A_s}^2$, we conclude that

$$\langle\sigma v\rangle_{x_F}^{A_s A_s} \simeq \frac{v_F^2 \kappa^4}{48\pi m_{\tilde{\chi}_1^0}^2} \quad (2.28)$$

and

$$|\kappa| \sim 0.40 \times \left(\frac{m_{\tilde{\chi}_1^0}}{300 \text{ GeV}} \right)^{1/2} \quad (2.29)$$

to predict the observed density.

3. $\tilde{\chi}_1^0 \tilde{\chi}_1^0 \rightarrow h_s A_s$

This process occurs if $2m_{\tilde{\chi}_1^0} > m_{h_s} + m_{A_s}$ and proceeds through the s -channel exchange of Z and CP-odd Higgs bosons and the t -channel exchange of neutralinos. Compared with the previous two annihilations, the full analytic expression

of $\langle\sigma v\rangle_{x_F}^{h_s A_s}$ is much more complex [70]. However, given that the contributions from the exchanges of A_s and $\tilde{\chi}_1^0$ are dominant for the small λ and sizable $|\kappa|$ case, it can be simplified as follows [5, 69]

$$\langle\sigma v\rangle_{x_F}^{h_s A_s} \simeq \frac{1}{64\pi m_{\tilde{\chi}_1^0}^2} \left\{ \left[1 - \frac{(m_{h_s} + m_{A_s})^2}{4m_{\tilde{\chi}_1^0}^2} \right] \left[1 - \frac{(m_{h_s} - m_{A_s})^2}{4m_{\tilde{\chi}_1^0}^2} \right] \right\}^{1/2} |\mathcal{A}_s + \mathcal{A}_t|^2,$$

where the s - and t -channel contributions are approximated by

$$\begin{aligned} \mathcal{A}_s &\simeq \frac{-2m_{\tilde{\chi}_1^0} C_{\tilde{\chi}_1^0 \tilde{\chi}_1^0 A_s} C_{h_s A_s A_s}}{m_{A_s}^2 - 4m_{\tilde{\chi}_1^0}^2}, \\ \mathcal{A}_t &\simeq -2C_{\tilde{\chi}_1^0 \tilde{\chi}_1^0 h_s} C_{\tilde{\chi}_1^0 \tilde{\chi}_1^0 A_s} \left[1 + \frac{2m_{A_s}^2}{4m_{\tilde{\chi}_1^0}^2 - (m_{h_s}^2 + m_{A_s}^2)} \right], \end{aligned} \quad (2.30)$$

respectively, assuming that h_s is not exceptionally light to forbid A_s -mediated resonant annihilation. Furthermore, from the formula of $C_{h_s A_s A_s}$ in Eq. (2.21), one can infer that if $|m_{\tilde{\chi}_1^0} - A_\kappa| \ll (4m_{\tilde{\chi}_1^0}^2 - m_{A_s}^2)/|m_{\tilde{\chi}_1^0}|$, $|\mathcal{A}_t|$ is much larger than $|\mathcal{A}_s|$, reflecting that the t -channel contribution prevails. In this case, $\langle\sigma v\rangle_{x_F}^{h_s A_s}$ is simplified as

$$\langle\sigma v\rangle_{x_F}^{h_s A_s} \simeq \frac{\kappa^4}{4\pi m_{\tilde{\chi}_1^0}^2}, \quad (2.31)$$

if $|m_{\tilde{\chi}_1^0}|$ is much larger than m_{A_s} and m_{h_s} , and

$$|\kappa| \sim 0.15 \times \left(\frac{m_{\tilde{\chi}_1^0}}{300 \text{ GeV}} \right)^{1/2} \quad (2.32)$$

to predict the observed density.

Notably, once the process $\tilde{\chi}_1^0 \tilde{\chi}_1^0 \rightarrow h_s A_s$ is kinematically allowed, at least one of the annihilations $\tilde{\chi}_1^0 \tilde{\chi}_1^0 \rightarrow h_s h_s$ and $\tilde{\chi}_1^0 \tilde{\chi}_1^0 \rightarrow A_s A_s$ is open. Since the former channel is dominated by s-wave contributions while the latter ones are p-wave processes, $\tilde{\chi}_1^0 \tilde{\chi}_1^0 \rightarrow h_s A_s$ dominantly contributes to $\langle\sigma v\rangle_{x_F}$. Additionally, the annihilation $\tilde{\chi}_1^0 \tilde{\chi}_1^0 \rightarrow h A_s$, which proceeds in a manner similar to $\tilde{\chi}_1^0 \tilde{\chi}_1^0 \rightarrow h_s A_s$, may provide substantial contributions to $\langle\sigma v\rangle_{x_F}$ when λ and V_h^S take exceptionally large values. Such a possibility, however, has been rigorously bounded by the results of the LZ experiment and the measurements of Higgs property at the LHC.

To achieve the observed relic abundance, the Singlino-dominated DM can also co-annihilate with electroweakinos. Corresponding processes include $\tilde{\chi}_i \tilde{\chi}_i$, $\tilde{\chi}_i \tilde{\chi}_j$, $\tilde{\chi}_j \tilde{\chi}_j \rightarrow XX'$, where $\tilde{\chi}_i$ and $\tilde{\chi}_j$ denote either the LSP or next-to-lightest supersymmetric particle (NLSP) and XX' represents SM particles. Basically, these annihilations influence the abundance only when the mass difference between $\tilde{\chi}_1^0$ and its co-annihilation partner is less than approximately 10% [69, 72], which necessitates the tuning of the two theoretically independent masses and thus leads to the suppression of Bayesian evidence.

2.3.2 DM-nucleon scattering

In the regime of heavy squarks, the SI scattering of DM with nucleons predominantly arises from the t -channel exchange of CP -even Higgs bosons. The cross section takes the following form [67, 73]

$$\sigma_N^{\text{SI}} = \frac{4\mu_r^2}{\pi} |f^N|^2, \quad f^N = \sum_i^3 f_{h_i}^N = \sum_i^3 \frac{C_{\tilde{\chi}_1^0 \tilde{\chi}_1^0 h_i} C_{NNh_i}}{2m_{h_i}^2}, \quad (2.33)$$

where $N = p, n$ denotes a proton (p) or neutron (n), and $\mu_r \equiv m_N m_{\tilde{\chi}_1^0} / (m_N + m_{\tilde{\chi}_1^0})$ is the reduced mass of the DM-nucleon composite. C_{NNh_i} represents the strength of Higgs coupling to the nucleon, given by

$$C_{NNh_i} = -\frac{m_N}{v} \left[F_d^N (V_{h_i}^{\text{SM}} - \tan \beta V_{h_i}^{\text{NSM}}) + F_u^N \left(V_{h_i}^{\text{SM}} + \frac{1}{\tan \beta} V_{h_i}^{\text{NSM}} \right) \right]. \quad (2.34)$$

Here, F_d^N and F_u^N are defined as $F_d^N \equiv f_d^{(N)} + f_s^{(N)} + \frac{2}{27} f_G^{(N)}$ and $F_u^N \equiv f_u^{(N)} + \frac{4}{27} f_G^{(N)}$, where the nucleon form factors $f_q^{(N)} \equiv m_N^{-1} \langle N | m_q q \bar{q} | N \rangle$ for $q = u, d, s$ denote the normalized light quark contribution to the nucleon mass and $f_G^{(N)} \equiv 1 - \sum_{q=u,d,s} f_q^{(N)}$ represents other heavy quarks' mass fraction in the nucleon [74, 75]. For the default settings of the package micrOMEGAs for $f_q^{(N)}$ [76–78], $F_u^p \simeq F_u^n \simeq 0.15$, $F_d^p \simeq F_d^n \simeq 0.13$, and therefore, $\sigma_{\tilde{\chi}_1^0-p}^{\text{SI}} \simeq \sigma_{\tilde{\chi}_1^0-n}^{\text{SI}}$.

Because the H -mediated contribution to σ_N^{SI} usually plays a minor role², we focus on the contribution from the t -channel exchange of the SM-like Higgs boson h and the singlet Higgs boson h_s . Using the formulas from Eqs.(2.14)–(2.20), we obtain the couplings $C_{\tilde{\chi}_1^0 \tilde{\chi}_1^0 h}$ and $C_{\tilde{\chi}_1^0 \tilde{\chi}_1^0 h_s}$ for the Singlino-dominated $\tilde{\chi}_1^0$ as follows:

$$C_{\tilde{\chi}_1^0 \tilde{\chi}_1^0 h} \simeq \frac{\mu_{\text{tot}}}{v} \left(\frac{\lambda v}{\mu_{\text{tot}}} \right)^2 \frac{Z_s V_h^{\text{SM}} (m_{\tilde{\chi}_1^0} / \mu_{\text{tot}} - \sin 2\beta)}{1 - (m_{\tilde{\chi}_1^0} / \mu_{\text{tot}})^2} + \frac{\lambda}{2\sqrt{2}} \left(\frac{\lambda v}{\mu_{\text{tot}}} \right)^2 \frac{Z_s V_h^{\text{S}} \sin 2\beta}{[1 - (m_{\tilde{\chi}_1^0} / \mu_{\text{tot}})^2]} - \sqrt{2} \kappa Z_s V_h^{\text{S}} \left[1 + \left(\frac{\lambda v}{\sqrt{2} \mu_{\text{tot}}} \right)^2 \frac{1}{1 - (m_{\tilde{\chi}_1^0} / \mu_{\text{tot}})^2} \frac{\mu_{\text{eff}}}{\mu_{\text{tot}}} \right], \quad (2.35)$$

$$C_{\tilde{\chi}_1^0 \tilde{\chi}_1^0 h_s} \simeq \frac{\mu_{\text{tot}}}{v} \left(\frac{\lambda v}{\mu_{\text{tot}}} \right)^2 \frac{Z_s V_{h_s}^{\text{SM}} (m_{\tilde{\chi}_1^0} / \mu_{\text{tot}} - \sin 2\beta)}{1 - (m_{\tilde{\chi}_1^0} / \mu_{\text{tot}})^2} + \frac{\lambda}{2\sqrt{2}} \left(\frac{\lambda v}{\mu_{\text{tot}}} \right)^2 \frac{Z_s V_{h_s}^{\text{S}} \sin 2\beta}{[1 - (m_{\tilde{\chi}_1^0} / \mu_{\text{tot}})^2]} - \sqrt{2} \kappa Z_s V_{h_s}^{\text{S}} \left[1 + \left(\frac{\lambda v}{\sqrt{2} \mu_{\text{tot}}} \right)^2 \frac{1}{1 - (m_{\tilde{\chi}_1^0} / \mu_{\text{tot}})^2} \frac{\mu_{\text{eff}}}{\mu_{\text{tot}}} \right], \quad (2.36)$$

and the expression of the SI cross section is [49]

$$\sigma_{\tilde{\chi}_1^0-N}^{\text{SI}} \simeq 5 \times 10^{-45} \text{ cm}^2 \left(\frac{\mathcal{A}}{0.1} \right)^2, \quad (2.37)$$

²This contribution is proportional to $\tan^2 \beta / m_H^4$ and is typically less than 10^{-49} cm^2 for $\tan \beta \leq 5$, as indicated by Figure 6 of [5]. With the further increase of $\tan \beta$, m_H is stringently limited by the LHC search for extra Higgs bosons (see, e.g., Figure 22 of [79] for the MSSM results.). Consequently, the contribution has difficulty reaching 10^{-47} cm^2 . Therefore, barring the blind spots discussed in [80], it is less crucial.

where

$$\mathcal{A} = \left(\frac{125\text{GeV}}{m_h} \right)^2 V_h^{\text{SM}} C_{\tilde{\chi}_1^0 \tilde{\chi}_1^0 h} + \left(\frac{125\text{GeV}}{m_{h_s}} \right)^2 V_{h_s}^{\text{SM}} C_{\tilde{\chi}_1^0 \tilde{\chi}_1^0 h_s}. \quad (2.38)$$

Given the approximations of V_h^{S} and $V_{h_s}^{\text{SM}}$ in Eq. (2.11), these formulas suggest that the primary contribution to \mathcal{A} in the series expansion of λ is proportional to $\lambda\kappa$ if the singlet–doublet mixing is substantial and the contribution mediated by h significantly cancels out that mediated by h_s . This dynamic is critical only when h_s is moderately light. In contrast, if h_s is tremendously massive and consequently h is purely SM like (i.e., $V_h^{\text{SM}} \simeq 1$, $V_h^{\text{S}} \simeq 0$, and $V_{h_s}^{\text{SM}} \simeq 0$), \mathcal{A} 's expression is significantly simplified:

$$\mathcal{A} = \left(\frac{125\text{GeV}}{m_h} \right)^2 \frac{\mu_{\text{tot}}}{v} \left(\frac{\lambda v}{\mu_{\text{tot}}} \right)^2 \frac{Z_s(m_{\tilde{\chi}_1^0}/\mu_{\text{tot}} - \sin 2\beta)}{1 - (m_{\tilde{\chi}_1^0}/\mu_{\text{tot}})^2}, \quad (2.39)$$

indicating that \mathcal{A} is proportional to λ^4 . Either a small λ or the correlation $m_{\tilde{\chi}_1^0}/\mu_{\text{tot}} \simeq \sin 2\beta$, known as the blind-spot condition of the NMSSM [81], is required to suppress the SI cross section.

Regarding the spin-dependent (SD) scattering cross section, only the t -channel exchange of a Z boson contributes in the limit of very massive squarks. It is approximated by [66, 67]

$$\sigma_{\tilde{\chi}_1^0-N}^{\text{SD}} \simeq C_N \times 10^{-4} \text{ pb} \times \left(\frac{N_{13}^2 - N_{14}^2}{0.1} \right)^2, \quad (2.40)$$

$$\simeq C_N \times 10^{-2} \text{ pb} \times \left(\frac{\lambda v}{\sqrt{2}\mu_{\text{tot}}} \right)^4 \left(\frac{N_{15}^2 \cos 2\beta}{1 - (m_{\tilde{\chi}_1^0}/\mu_{\text{tot}})^2} \right)^2, \quad (2.41)$$

where $C_N \simeq 4.0$ for protons and $C_N \simeq 3.1$ for neutrons. This formula indicates that the SD cross section is proportional to $(\lambda v/\mu_{\text{tot}})^4$ and increases as $m_{\tilde{\chi}_1^0}$ approaches μ_{tot} from below. It is the same as the expression of the SD scattering cross section for Bino-dominated DM,

$$\sigma_{\tilde{B}_1^0-N}^{\text{SD}} \simeq C_N \times 10^{-2} \text{ pb} \times \left(\frac{v}{\sqrt{2}\mu_{\text{tot}}} \right)^4 \left(\frac{\cos 2\beta}{1 - (m_{\tilde{\chi}_1^0}/\mu_{\text{tot}})^2} \right)^2, \quad (2.42)$$

except for an additional factor $\lambda^4 N_{15}^2$.

In summary, the aforementioned formulas suggest the plausible existence of a secluded DM sector, composed of singlet states [51]. Specifically, the Singlino-dominated DM achieves the observed relic abundance primarily through the processes $\tilde{\chi}_1^0 \tilde{\chi}_1^0 \rightarrow h_s A_s, h_s h_s, A_s A_s$, or h_s/A_s -funnel by tuning κ . Since the DM sector communicates with the SM sector mainly by the weak singlet–doublet Higgs mixing, the DM-nucleon scattering is suppressed by λ .

3 Numerical results

Here the sampling strategy of this study is introduced and the features of DM physics in the GNMSSM are demonstrated. The model file of the GNMSSM was generated by the package **SARAH** 4.14.3 [82–85], the particle spectrum and low-energy flavor measurements were calculated using the **SPheno** 4.0.4 [86, 87] and **FlavorKit** [88] code, respectively, and DM observables were computed with the package **micrOMEGAs** 5.0.4 [89–94]. We analyzed the acquired samples using the marginal posterior probability density function (PDF) in Bayesian inference and the profile likelihood (PL) in frequentist statistics [95]³.

3.1 Research strategy

We started by constructing a likelihood function that incorporated the DM relic abundance, results from the LZ experiment [9], and other relevant constraints on the GNMSSM. The likelihood function is given by

$$\begin{aligned}\mathcal{L} &\equiv \mathcal{L}_{\Omega h^2} \times \mathcal{L}_{\text{LZ}} \times \mathcal{L}_{\text{Const}}, \\ \mathcal{L}_{\Omega h^2} &= \exp \left[-\frac{1}{2} \left(\frac{\Omega h^2 - 0.120}{0.012} \right)^2 \right], \quad \mathcal{L}_{\text{LZ}} = \exp \left[-\frac{\sigma_{\tilde{\chi}_1^0 - p}^{\text{SI}}}{2\delta_\sigma^2} \right], \\ \mathcal{L}_{\text{Const}} &= \begin{cases} 1 & \text{if satisfying all experimental constraints} \\ \exp[-100] & \text{otherwise} \end{cases}. \end{aligned} \quad (3.3)$$

In this formulation, we assumed the relic abundance Ωh^2 followed a Gaussian distribution. We used its central value from the Planck experiment [2] with a theoretical uncertainty of 10% in its calculation. Regarding the likelihood function of the LZ experiment, \mathcal{L}_{LZ} , we modeled it with a Gaussian distribution centered at zero and defined $\delta_\sigma^2 = \text{UL}_\sigma^2/1.64^2 + (0.2\sigma)^2$, where UL_σ refers to the upper limit of the LZ results on the DM-nucleon SI scattering rate at a 90% C. L., and 0.2σ accounts for theoretical uncertainties [96]. $\mathcal{L}_{\text{Const}}$ includes the following experimental constraints:

³In frequentist statistics, the one-dimensional PL refers to the maximum likelihood value in a specific parameter space [95]. For a given set of input parameters $\Theta \equiv (\Theta_1, \Theta_2, \dots)$, the one-dimensional PL, denoted as

$$\mathcal{L}(\Theta_A) = \max_{\Theta_1, \dots, \Theta_{A-1}, \Theta_{A+1}, \dots} \mathcal{L}(\Theta), \quad (3.1)$$

is obtained by maximizing the likelihood function while varying the other parameters. At a given point Θ_A , $\mathcal{L}(\Theta_A)$ reflects the capability of that point within the theory to explain the experimental data. The one-dimensional marginal posterior PDF is derived through the integration of the posterior PDF from the Bayesian theorem with respect to the remaining inputs of the model, i.e.,

$$P(\Theta_A) = \int P(\Theta) d\Theta_1 d\Theta_2 \dots d\Theta_{A-1} d\Theta_{A+1} \dots \quad (3.2)$$

The PL reflects the data’s preference for the parameter space, while the posterior PDF represents the preference of the samples obtained during the scan.

Table 1. In this study, the parameter space was explored for the h_1 scenario, assuming all the inputs were flatly distributed in the prior since they have clear physical meanings in the small λ case. We assumed that the soft trilinear coefficients for the third-generation squarks were equal, i.e., $A_t = A_b$, for simplicity and let them vary because they could significantly influence the Standard Model (SM)-like Higgs boson mass by radiative corrections. We also fixed $M_3 = 3$ TeV and selected a shared value of 2 TeV for the other unmentioned dimensional parameters to be consistent with the Large Hadron Collider (LHC) search for new physics, noting that they are not crucial to this study. We define all these parameters at the renormalization scale $Q_{inp} = 1$ TeV. **The h_2 scenario corresponds to the same parameter space as that of the h_1 scenario except that $1 \text{ GeV} \leq m_B \leq 130 \text{ GeV}$.**

Parameter	Prior	Range	Parameter	Prior	Range
λ	Flat	0–0.75	κ	Flat	−0.75–0.75
$\tan \beta$	Flat	1–60	v_s/TeV	Flat	10^{-3} –1.0
$\mu_{\text{tot}}/\text{TeV}$	Flat	0.1–1.0	m_N/TeV	Flat	−1.0–1.0
m_B/TeV	Flat	0.1–1.0	m_C/TeV	Flat	10^{-3} –1.0
M_1/TeV	Flat	−1.0–1.0	M_2/TeV	Flat	0.1–1.0
A_t/TeV	Flat	−5.0–5.0	A_λ/TeV	Flat	−2.5–2.5

- **Higgs data fit:** The properties of the SM-like Higgs boson h must align with the LHC Higgs data at a 95% confidence level. This condition was examined using the `HiggsSignal 2.6.2` code, requiring the fit’s p -value to exceed 0.05 [97–100].
- **Extra Higgs searches:** This aspect was tested using the `HiggsBounds 5.10.2` code to conduct a comprehensive search for additional Higgs bosons beyond the SM at LEP, Tevatron, and the LHC [101–105].
- **Indirect DM searches:** The Fermi-LAT collaboration has made years of observations of dwarf galaxies, limiting the annihilation cross section as a function of the DM mass⁴. We employed the likelihood function proposed in Ref. [106, 107] to implement this constraint.
- **B -physics observables:** The branching ratios of $B_s \rightarrow \mu^+\mu^-$ and $B \rightarrow X_s\gamma$ should remain consistent with their experimental measurements at the 2σ level [108].
- **Vacuum stability:** The vacuum state of the scalar potential should be either stable or long lived [53]. This criterion was rigorously examined using `VevaciousPlusPlus` [109], the C++ version of `Vevacious` [110]. Note that its implications on the GNMSSM were comprehensively addressed in a recent study [53].

⁴see website: www-glast.stanford.edu/pub_data/1048

Table 2. Experimental analyses included in the package **SModelS-2.1.1**.

Name	Scenario	Final State	Luminosity(fb ⁻¹)
CMS-SUS-17-010 [111]	$\tilde{\chi}_1^\pm \tilde{\chi}_1^\mp \rightarrow W^\pm \tilde{\chi}_1^0 W^\mp \tilde{\chi}_1^0$ $\tilde{\chi}_1^\pm \tilde{\chi}_1^\mp \rightarrow \nu \bar{\ell} \bar{\nu}$	$2\ell + E_T^{\text{miss}}$	35.9
CMS-SUS-17-009 [112]	$\bar{\ell}\bar{\ell} \rightarrow \ell \tilde{\chi}_1^0 \ell \tilde{\chi}_1^0$	$2\ell + E_T^{\text{miss}}$	35.9
CMS-SUS-17-004 [113]	$\tilde{\chi}_2^0 \tilde{\chi}_1^\pm \rightarrow Wh(Z) \tilde{\chi}_1^0 \tilde{\chi}_1^\pm$	$n\ell(n \geq 0) + n\bar{j}(n \geq 0) + E_T^{\text{miss}}$	35.9
CMS-SUS-16-045 [114]	$\tilde{\chi}_2^0 \tilde{\chi}_1^\pm \rightarrow W^\pm \tilde{\chi}_1^0 h \tilde{\chi}_1^\pm$	$1\ell \text{ } 2b + E_T^{\text{miss}}$	35.9
CMS-SUSY-16-039 [115]	$\tilde{\chi}_2^0 \tilde{\chi}_1^\pm \rightarrow \ell \bar{\nu} \ell \bar{\ell}$	$n\ell(n > 0)(\tau) + E_T^{\text{miss}}$	35.9
	$\tilde{\chi}_2^0 \tilde{\chi}_1^\pm \rightarrow \bar{\tau} \nu \bar{\ell} \ell$		
	$\tilde{\chi}_2^0 \tilde{\chi}_1^\pm \rightarrow \bar{\tau} \nu \bar{\tau} \tau$		
	$\tilde{\chi}_2^0 \tilde{\chi}_1^\pm \rightarrow WZ \tilde{\chi}_1^0 \tilde{\chi}_1^\pm$		
	$\tilde{\chi}_2^0 \tilde{\chi}_1^\pm \rightarrow WH \tilde{\chi}_1^0 \tilde{\chi}_1^\pm$		
CMS-SUS-16-034 [116]	$\tilde{\chi}_2^0 \tilde{\chi}_1^\pm \rightarrow W \tilde{\chi}_1^0 Z(h) \tilde{\chi}_1^\pm$	$n\ell(n \geq 2) + n\bar{j}(n \geq 1) E_T^{\text{miss}}$	35.9
ATLAS-1803-02762 [117]	$\tilde{\chi}_2^0 \tilde{\chi}_1^\pm \rightarrow WZ \tilde{\chi}_1^0 \tilde{\chi}_1^\pm$	$n\ell(n \geq 2) + E_T^{\text{miss}}$	36.1
	$\tilde{\chi}_2^0 \tilde{\chi}_1^\pm \rightarrow \nu \bar{\ell} \ell \bar{\ell}$		
	$\tilde{\chi}_1^\pm \tilde{\chi}_1^\mp \rightarrow \nu \bar{\ell} \nu \bar{\ell}$		
	$\bar{\ell}\bar{\ell} \rightarrow \ell \tilde{\chi}_1^0 \ell \tilde{\chi}_1^0$		
ATLAS-1812-09432 [118]	$\tilde{\chi}_2^0 \tilde{\chi}_1^\pm \rightarrow Wh \tilde{\chi}_1^0 \tilde{\chi}_1^\pm$	$n\ell(n \geq 0) + n\bar{j}(n \geq 0) + n\bar{b}(n \geq 0) + n\gamma(n \geq 0) + E_T^{\text{miss}}$	36.1
ATLAS-1806-02293 [119]	$\tilde{\chi}_2^0 \tilde{\chi}_1^\pm \rightarrow WZ \tilde{\chi}_1^0 \tilde{\chi}_1^\pm$	$n\ell(n \geq 2) + n\bar{j}(n \geq 0) + E_T^{\text{miss}}$	36.1
ATLAS-1912-08479 [120]	$\tilde{\chi}_2^0 \tilde{\chi}_1^\pm \rightarrow W(\rightarrow l\nu) \tilde{\chi}_1^0 Z(\rightarrow \ell\ell) \tilde{\chi}_1^\pm$	$3\ell + E_T^{\text{miss}}$	139
ATLAS-1908-08215 [121]	$\bar{\ell}\bar{\ell} \rightarrow \ell \tilde{\chi}_1^0 \ell \tilde{\chi}_1^0$ $\tilde{\chi}_1^\pm \tilde{\chi}_1^\mp$	$2\ell + E_T^{\text{miss}}$	139
ATLAS-1909-09226 [122]	$\tilde{\chi}_2^0 \tilde{\chi}_1^\pm \rightarrow Wh \tilde{\chi}_1^0 \tilde{\chi}_1^\pm$	$1\ell + h(\rightarrow b\bar{b}) + E_T^{\text{miss}}$	139

Next, we performed sophisticated scans over the parameter space in Table 1 for the h_1 and h_2 scenario⁵, using the MultiNest algorithm with $n\text{live} = 8000$ [132]⁶ and the likelihood function in Eq. (3.3). Regarding the acquired samples, we were particularly interested in those that can explain the relic abundance at the 2σ level, satisfy the LZ bounds, and be consistent with all the experimental constraints. We

⁵Given that the DM physics of the GNMSSM involves numerous free parameters and ξ' only appears in the tadpole equation to determine the soft squared mass m_S^2 , we simplify our study by assuming that the tadpole term in Eq. (2.2) vanishes. Under this assumption, A_κ is related to v_s by the equation $\kappa A_\kappa = \sqrt{2}m_B^2/v_s + \lambda\mu v^2/v_s^2 - \lambda(A_\lambda + m_N - \sqrt{2}\sin 2\beta\kappa v_s)v^2/(2v_s^2) + \sqrt{2}\kappa^2 v_s - 3\kappa m_N$, according to the expression of ξ' in Eq. (2.9). As we will demonstrate below, this specific parameter configuration suggests that the GNMSSM predominantly predicts a Singlino-dominated DM. We emphasize that this conclusion remains valid even when A_κ is considered a free parameter, leading to a nonzero ξ' . The primary reason for this is that A_κ only influences the triple Higgs couplings in Eq. (2.21), and allowing it to vary freely enables the theory to more easily achieve the observed relic abundance when any of the processes $\tilde{\chi}_1^0 \tilde{\chi}_1^0 \rightarrow h_s A_s, h_s h_s, A_s A_s$ is the dominant annihilation channel. We verified that κA_κ in this study is within a reasonable range, satisfying $-800 \text{ GeV} \lesssim \kappa A_\kappa \lesssim 1200 \text{ GeV}$ for the 2σ credible region.

⁶ $N\text{live}$ in the MultiNest method represents the number of active or live points to determine the iso-likelihood contour in each iteration [132, 133]. The larger it is, the more detailed the scan results will be in surveying the parameter space.

Table 3. Experimental analyses of the electroweakino production processes considered in this study, categorized by the topologies of the electroweakino's signal.

Scenario	Final State	Name
$\tilde{\chi}_2^0 \tilde{\chi}_1^\pm \rightarrow WZ \tilde{\chi}_1^0 \tilde{\chi}_1^0$	$n\ell(n \geq 2) + nj(n \geq 0) + E_T^{\text{miss}}$	CMS-SUS-20-001 (137 fb ⁻¹) [123]
		ATLAS-2106-01676 (139 fb ⁻¹) [124]
		CMS-SUS-17-004 (35.9 fb ⁻¹) [113]
		CMS-SUS-16-039 (35.9 fb ⁻¹) [115]
		ATLAS-1803-02762 (36.1 fb ⁻¹) [117]
		ATLAS-1806-02293 (36.1 fb ⁻¹) [119]
$\tilde{\chi}_2^0 \tilde{\chi}_1^\pm \rightarrow \ell \tilde{\nu} \tilde{\ell}$	$n\ell(n = 3) + E_T^{\text{miss}}$	CMS-SUS-16-039 (35.9 fb ⁻¹) [115]
		ATLAS-1803-02762 (36.1 fb ⁻¹) [117]
$\tilde{\chi}_2^0 \tilde{\chi}_1^\pm \rightarrow \tilde{\tau} \nu \tilde{\ell}$	$2\ell + 1\tau + E_T^{\text{miss}}$	CMS-SUS-16-039 (35.9 fb ⁻¹) [115]
$\tilde{\chi}_2^0 \tilde{\chi}_1^\pm \rightarrow \tilde{\tau} \nu \tilde{\tau} \tau$	$3\tau + E_T^{\text{miss}}$	CMS-SUS-16-039 (35.9 fb ⁻¹) [115]
$\tilde{\chi}_2^0 \tilde{\chi}_1^\pm \rightarrow Wh \tilde{\chi}_1^0 \tilde{\chi}_1^0$	$n\ell(n \geq 1) + nb(n \geq 0) + nj(n \geq 0) + E_T^{\text{miss}}$	ATLAS-1909-09226 (139 fb ⁻¹) [125]
		CMS-SUS-17-004 (35.9 fb ⁻¹) [113]
		CMS-SUS-16-039 (35.9 fb ⁻¹) [115]
		ATLAS-1812-09432 (36.1 fb ⁻¹) [118]
		CMS-SUS-16-034 (35.9 fb ⁻¹) [116]
		CMS-SUS-16-045 (35.9 fb ⁻¹) [114]
$\tilde{\chi}_1^\mp \tilde{\chi}_1^\pm \rightarrow WW \tilde{\chi}_1^0 \tilde{\chi}_1^0$	$2\ell + E_T^{\text{miss}}$	ATLAS-1908-08215 (139 fb ⁻¹) [121]
		CMS-SUS-17-010 (35.9 fb ⁻¹) [111]
$\tilde{\chi}_1^\mp \tilde{\chi}_1^\pm \rightarrow 2\tilde{\ell} \nu(\tilde{\nu} \ell)$	$2\ell + E_T^{\text{miss}}$	ATLAS-1908-08215 (139 fb ⁻¹) [121]
		CMS-SUS-17-010 (35.9 fb ⁻¹) [111]
$\tilde{\chi}_2^0 \tilde{\chi}_1^\pm \rightarrow ZW \tilde{\chi}_1^0 \tilde{\chi}_1^0$ $\tilde{\chi}_1^\pm \tilde{\chi}_1^\mp \rightarrow WW \tilde{\chi}_1^0 \tilde{\chi}_1^0$	$2j(\text{large}) + E_T^{\text{miss}}$	ATLAS-2108-07586 (139 fb ⁻¹) [126]
$\tilde{\chi}_2^0 \tilde{\chi}_1^\pm \rightarrow (h/Z)W \tilde{\chi}_1^0 \tilde{\chi}_1^0$ $\tilde{\chi}_2^0 \tilde{\chi}_3^0 \rightarrow (h/Z)Z \tilde{\chi}_1^0 \tilde{\chi}_1^0$	$j(\text{large}) + b(\text{large}) + E_T^{\text{miss}}$	ATLAS-2108-07586 (139 fb ⁻¹) [126]
$\tilde{\chi}_2^0 \tilde{\chi}_1^\mp \rightarrow h/ZW \tilde{\chi}_1^0 \tilde{\chi}_1^0, \tilde{\chi}_1^0 \rightarrow \gamma/Z\tilde{G}$ $\tilde{\chi}_1^\pm \tilde{\chi}_1^\mp \rightarrow WW \tilde{\chi}_1^0 \tilde{\chi}_1^0, \tilde{\chi}_1^0 \rightarrow \gamma/Z\tilde{G}$	$2\gamma + n\ell(n \geq 0) + nb(n \geq 0) + nj(n \geq 0) + E_T^{\text{miss}}$	ATLAS-1802-03158 (36.1 fb ⁻¹) [127]
$\tilde{\chi}_2^0 \tilde{\chi}_1^\pm \rightarrow ZW \tilde{\chi}_1^0 \tilde{\chi}_1^0, \tilde{\chi}_1^0 \rightarrow h/Z\tilde{G}$ $\tilde{\chi}_1^\pm \tilde{\chi}_1^\mp \rightarrow WW \tilde{\chi}_1^0 \tilde{\chi}_1^0, \tilde{\chi}_1^0 \rightarrow h/Z\tilde{G}$ $\tilde{\chi}_2^0 \tilde{\chi}_1^0 \rightarrow Z \tilde{\chi}_1^0 \tilde{\chi}_1^0, \tilde{\chi}_1^0 \rightarrow h/Z\tilde{G}$ $\tilde{\chi}_1^\mp \tilde{\chi}_1^0 \rightarrow W \tilde{\chi}_1^0 \tilde{\chi}_1^0, \tilde{\chi}_1^0 \rightarrow h/Z\tilde{G}$	$n\ell(n \geq 4) + E_T^{\text{miss}}$	ATLAS-2103-11684 (139 fb ⁻¹) [128]
$\tilde{\chi}_i^{0,\pm} \tilde{\chi}_j^{0,\mp} \rightarrow \tilde{\chi}_1^0 \tilde{\chi}_1^0 + \chi_{\text{soft}} \rightarrow ZZ/H\tilde{G}\tilde{G}$	$n\ell(n \geq 2) + nb(n \geq 0) + nj(n \geq 0) + E_T^{\text{miss}}$	CMS-SUS-16-039 (35.9 fb ⁻¹) [115]
		CMS-SUS-17-004 (35.9 fb ⁻¹) [113]
		CMS-SUS-20-001 (137 fb ⁻¹) [123]
$\tilde{\chi}_i^{0,\pm} \tilde{\chi}_j^{0,\mp} \rightarrow \tilde{\chi}_1^0 \tilde{\chi}_1^0 + \chi_{\text{soft}} \rightarrow HH\tilde{G}\tilde{G}$	$n\ell(n \geq 2) + nb(n \geq 0) + nj(n \geq 0) + E_T^{\text{miss}}$	CMS-SUS-16-039 (35.9 fb ⁻¹) [115]
		CMS-SUS-17-004 (35.9 fb ⁻¹) [113]
$\tilde{\chi}_2^0 \tilde{\chi}_1^\pm \rightarrow W^* Z^* \tilde{\chi}_1^0 \tilde{\chi}_1^0$	$3\ell + E_T^{\text{miss}}$	ATLAS-2106-01676 (139 fb ⁻¹) [124]
$\tilde{\chi}_2^0 \tilde{\chi}_1^\pm \rightarrow Z^* W^* \tilde{\chi}_1^0 \tilde{\chi}_1^0$	$2\ell + nj(n \geq 0) + E_T^{\text{miss}}$	ATLAS-1911-12606 (139 fb ⁻¹) [129]
		ATLAS-1712-08119 (36.1 fb ⁻¹) [130]
		CMS-SUS-16-048 (35.9 fb ⁻¹) [131]
$\tilde{\chi}_2^0 \tilde{\chi}_1^\pm + \tilde{\chi}_1^\pm \tilde{\chi}_1^\mp + \tilde{\chi}_1^\pm \tilde{\chi}_1^0$	$2\ell + nj(n \geq 0) + E_T^{\text{miss}}$	ATLAS-1911-12606 (139 fb ⁻¹) [129]
		ATLAS-1712-08119 (36.1 fb ⁻¹) [130]
		CMS-SUS-16-048 (35.9 fb ⁻¹) [131]

Table 4. Primary annihilation channels for Singlino-dominated dark matter (DM) in the h_1 scenario and their marginal posterior probability density functions (PDFs) normalized to the total Bayesian evidence of the scenario. The second line takes into account all 21097 samples acquired from the scan, while the third line only includes those further satisfying the LHC constraints, which resulted in smaller PDFs than their corresponding ones in the second line. Regarding the co-annihilation in this table, the annihilation partners were Higgsino-like electroweakinos in most cases and Wino-like electroweakinos in a few cases, as indicated by the samples.

$\tilde{\chi}_1^0 \tilde{\chi}_1^0 \rightarrow h_s A_s$	$\tilde{\chi}_1^0 \tilde{\chi}_1^0 \rightarrow A_s A_s$	Co-annihilation	$\tilde{\chi}_1^0 \tilde{\chi}_1^0 \rightarrow h_s h_s$
58.1%	34.8%	2.5%	2.3%
58.0%	32.7%	2.4%	2.3%

will analyze their features using statistical quantities and illustrate the differences of the two scenarios.

Finally, we assessed the alignment of the samples with the results of the LHC search for electroweakinos. To reduce the calculation time, we initially utilized the program **SModelS-2.1.1** [134], which encoded various event-selection efficiencies by the topologies of the electroweakino signals listed in Table 2 to implement the task. Given that the exclusion capability of **SModelS-2.1.1** on the samples is limited by its database and strict working prerequisites, we further surveyed the surviving samples by simulating the analyses listed in Table 3. We finished this task by the following procedures. We concentrated on the electroweakino production processes

$$\begin{aligned}
pp &\rightarrow \tilde{\chi}_i^0 \tilde{\chi}_j^\pm, & i = 2, 3, 4, 5; & \quad j = 1, 2 \\
pp &\rightarrow \tilde{\chi}_i^\pm \tilde{\chi}_j^\mp, & i, j = 1, 2 \\
pp &\rightarrow \tilde{\chi}_i^0 \tilde{\chi}_j^0, & i, j = 2, 3, 4, 5
\end{aligned} \tag{3.4}$$

and calculated their cross sections to next-to-leading order using the program **Prospino2** [135]. Subsequently, we generated 10^5 events for these processes by **MadGraph_aMC@NLO** [136, 137] and furnished their parton shower and hadronization by the program **PYTHIA8** [138]. Detector simulations were implemented with the program **Delphes** [139]. Finally, we fed the event files into the package **CheckMATE-2.0.29** [140–142] to calculate the R value defined by $R \equiv \max\{S_i/S_{i,obs}^{95}\}$ for all the involved analyses, where S_i represents the simulated event number of the i -th signal region (SR), and $S_{i,obs}^{95}$ is the corresponding 95% confidence level upper limit. $R > 1$ means that the sample is experimentally excluded if the involved uncertainties are neglected [143], while $R < 1$ indicates that it is consistent with the experimental analyses.

3.2 Global features

By analyzing the samples acquired by the scans, we made the following observations:

Table 5. Similar to Table 4, but presenting the h_2 scenario results. The channel $\tilde{\chi}_1^0 \tilde{\chi}_1^0 \rightarrow q\bar{q}$ in this table proceeded primarily through exchanging a resonant h_s , A_s , or h .

$\tilde{\chi}_1^0 \tilde{\chi}_1^0 \rightarrow h_s h_s$	$\tilde{\chi}_1^0 \tilde{\chi}_1^0 \rightarrow h_s A_s$	Co-annihilation	$\tilde{\chi}_1^0 \tilde{\chi}_1^0 \rightarrow q\bar{q}$
42.3%	12.6%	5.9%	2.1%
18.3%	9.7%	4.1%	1.4%

- We obtained 21229 samples for the h_1 scenario and 20511 samples for the h_2 scenario. These sample sets accounted for the relic abundance at the 2σ level, remained consistent with the LZ bounds, and satisfied all the experimental constraints encoded in $\mathcal{L}_{\text{Const}}$. The Bayesian evidences were $\ln Z_{h_1} = -11.28 \pm 0.037$ and $\ln Z_{h_2} = -12.12 \pm 0.038$. The Jeffrey’s scale, defined as the ratio of $\ln Z_{h_1}$ to $\ln Z_{h_2}$, was equal to 0.84; thus, the h_1 scenario was better suited to account for experimental results than the h_2 scenario [48]. The primary reason was that the h_2 scenario introduced additional non-trivial theoretical constraints, specifically $m_B \lesssim 130$ GeV and $\lambda\mu_{\text{tot}} \lesssim 30$ GeV, based on the Higgs data fit of this analysis, leading to a more stringent limitation on its parameter space.
- The DM candidate may have been dominated by the Singlino or Bino field in its components. In the h_1 scenario, 21097 out of 21229 samples predicted a Singlino-dominated $\tilde{\chi}_1^0$, contributing to 99.3% of the Bayesian evidence. In contrast, 13113 out of 20511 samples in the h_2 scenario predicted a Singlino-dominated $\tilde{\chi}_1^0$, accounting for approximately 64.8% of the Bayesian evidence.
- After including constraints from the LHC search for supersymmetry, the sample numbers were reduced to 20709 and 12604 for the scenarios h_1 and h_2 , respectively. Correspondingly, the Bayesian evidences decreased by 2.4% and 38.8%, respectively. These results indicated that the LHC constraint had significant impacts on the DM physics of the h_2 scenario, but hardly affected that of the h_1 scenario.
- As discussed in Section 2.3.1, the relative importance between the annihilation channels $\tilde{\chi}_1^0 \tilde{\chi}_1^0 \rightarrow h_s h_s, A_s A_s, h_s A_s$ for the Singlino-dominated DM depended on the mass spectrum and couplings of the samples. We have categorized the samples based on their dominant annihilation processes and evaluated their impact on the Bayesian evidence. Tables 4 and 5 detail their contributions to the total Bayesian evidence for the h_1 and h_2 scenario, respectively, both before and after incorporating the LHC constraints. These tables reveal that most samples in the h_1 scenario predominantly annihilated through $\tilde{\chi}_1^0 \tilde{\chi}_1^0 \rightarrow h_s A_s$, aligning with the observed relic abundance. In contrast, the h_2 scenario showed

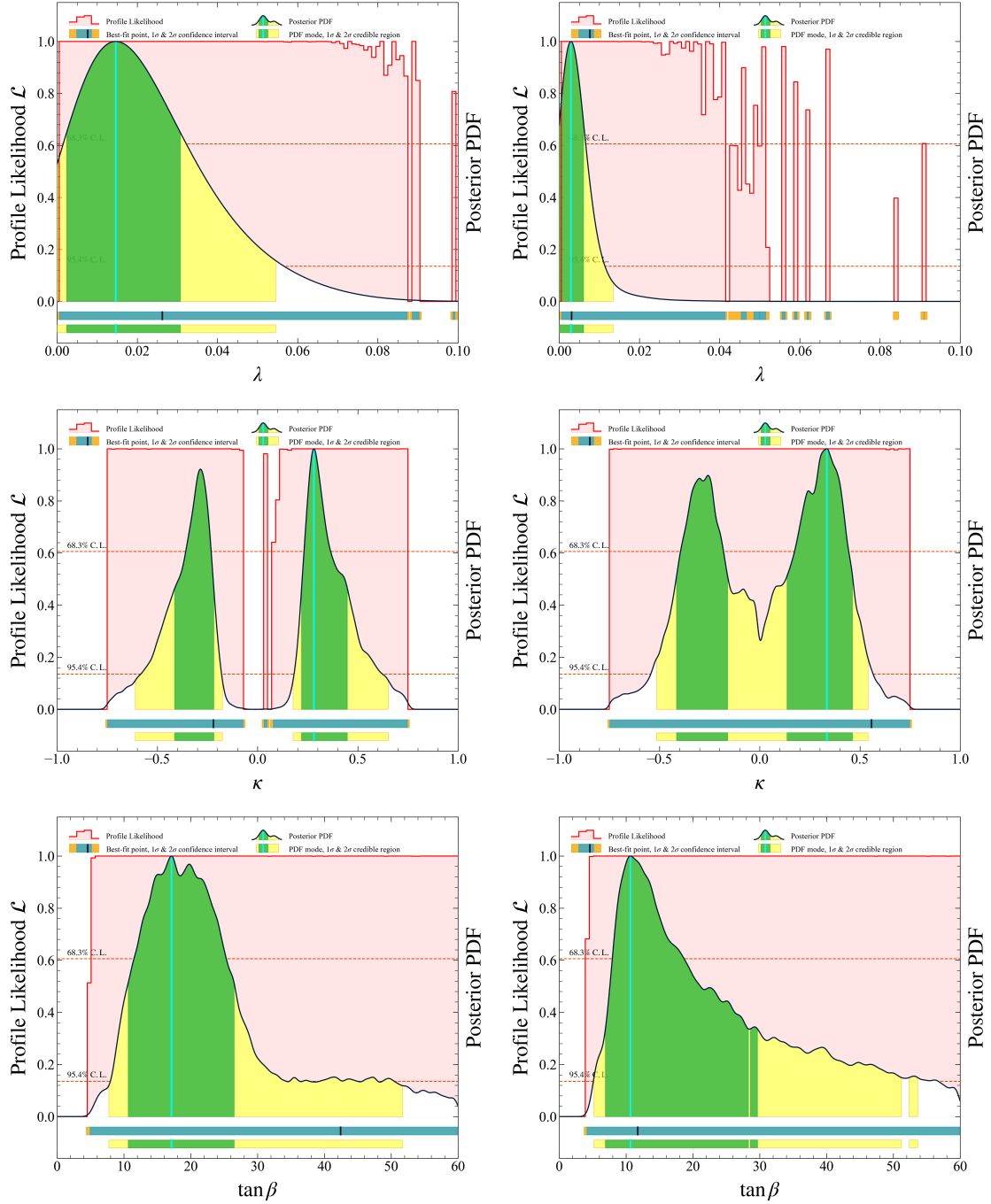


Figure 1. One-dimensional PLs (red line) and marginal posterior PDFs (black line) of λ , κ , and $\tan\beta$ before implementing the LHC constraints. The left panels show the results of the h_1 scenario, while the right panels depict those of the h_2 scenario. Statistical measures such as the confidence interval and credible region were introduced in Ref. [95].

that a substantial fraction of the samples primarily annihilated via $\tilde{\chi}_1^0 \tilde{\chi}_1^0 \rightarrow h_s h_s$, facing stringent restrictions from the LHC search for the supersymmetry.

- In the h_2 scenario, a significant fraction of samples predicted a Bino-dominated

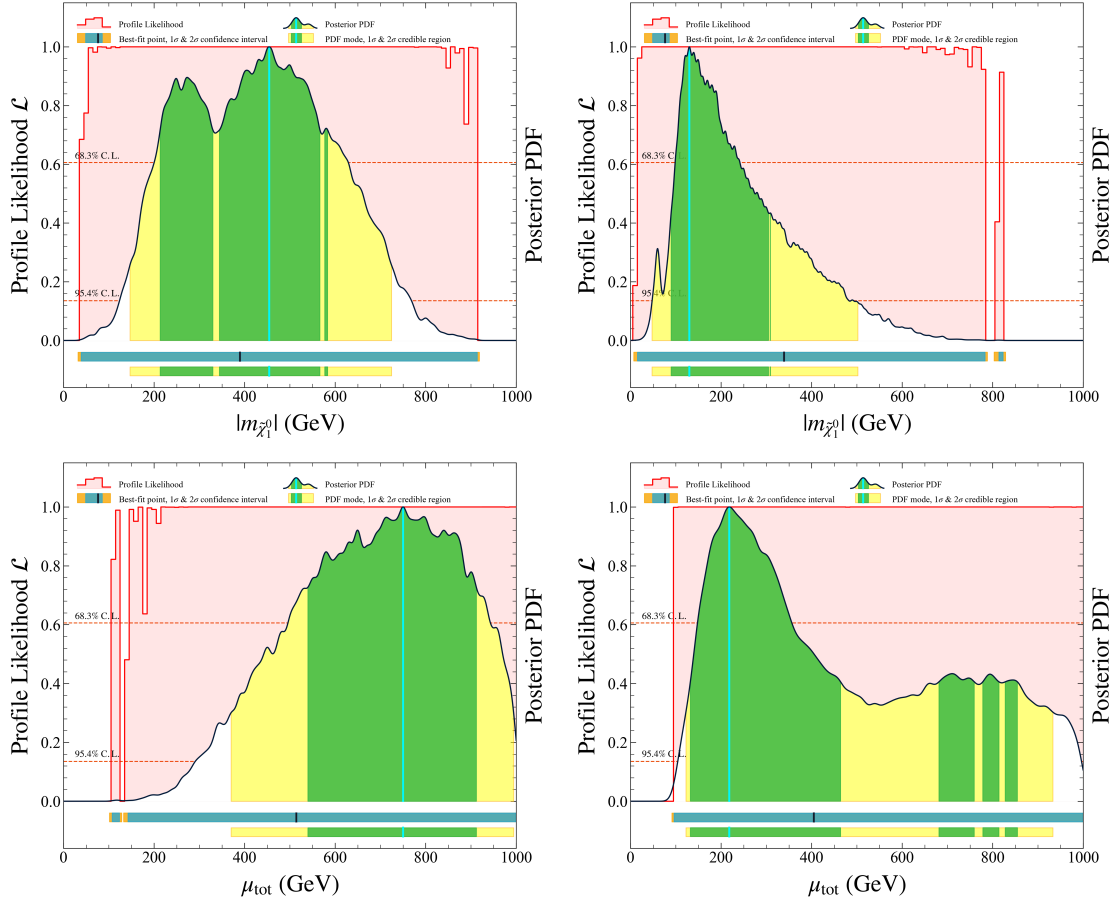


Figure 2. Same as Fig. 1, but for the distributions of $m_{\tilde{\chi}_1^0}$ and μ_{tot} .

$\tilde{\chi}_1^0$, accounting for 35.2% and 28.0% of the total Bayesian evidence before and after taking the LHC constraints into consideration, respectively. Such a DM achieved the observed relic abundance primarily through co-annihilating with Wino-like electroweakinos. It preferred a negative value of M_1 to suppress the SI DM-nucleon scattering by canceling different contributions [15]. The LZ experiment alone set a lower bound of approximately 380 GeV on μ_{tot} [19], and the LHC search for the compressed spectrum of supersymmetry by leptonic signals required $|m_{\tilde{\chi}_1^0}| \gtrsim 220$ GeV [124]. Our results confirmed these characteristics.

These aforementioned conclusions indicated that the GNMSSM preferred a Singlino-dominated DM, instead of a Bino-dominated DM, across a wide range of parameters. This feature distinguished it from the MSSM and \mathbb{Z}_3 -NMSSM.

In the analysis discussed below, we studied the statistical distributions of the input parameters that determined the property of $\tilde{\chi}_1^0$. We plotted one-dimensional PLs and marginal posterior PDFs of λ , κ , and $\tan\beta$ in Fig. 1 and those of $m_{\tilde{\chi}_1^0}$ and μ_{tot} in Fig. 2. The left panels in both figures show the results of the h_1 scenario

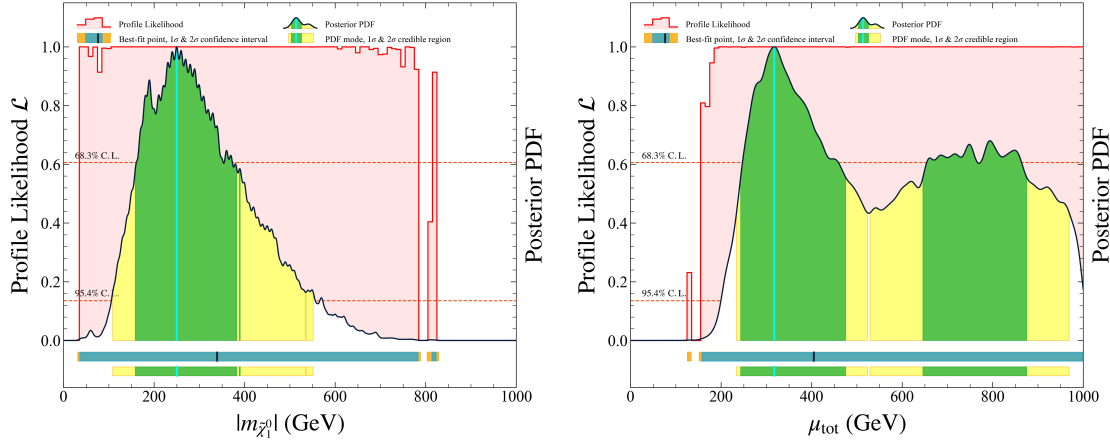


Figure 3. Same as Fig. 2, but for the results of the h_2 scenario after considering the LHC constraints.

without considering the LHC constraints, while the right panels depict those of the h_2 scenario. From these plots, several insights can be inferred:

- λ 's PL and posterior PDF distributions indicated that $\lambda \lesssim 0.09$ for almost all samples in the h_1 scenario and $\lambda \lesssim 0.05$ for almost all samples in the h_2 scenario. These ranges are notably narrower than those listed in Table 1, and the small values of λ are a distinctive feature of the GNMSSM. This trend primarily stemmed from the LZ constraint discussed in Section 2: in scenarios where $\tilde{\chi}_1^0$ is Singlino dominated, the main contribution to $\sigma_{\tilde{\chi}_1^0-N}^{\text{SI}}$ is proportional to $\lambda^2 \kappa^2$ for substantial singlet–doublet Higgs mixing and λ^4 in the heavy h_s limit. In contrast, when $\tilde{\chi}_1^0$ is Bino dominated, as significant in the h_2 scenario, the LZ constraint required μ_{tot} to exceed 380 GeV, and the Higgs data fit limited $\lambda \mu_{\text{tot}}$ in $\mathcal{M}_{\text{S},23}^2$ to approximately 30 GeV or less. In any scenario, a small λ is preferred.
- The value of κ varied widely from -0.75 to 0.75 . Notably, in the h_1 scenario, there were gaps around $\kappa = 0$ in the PL and posterior PDF distributions, while they were continuous in the h_2 scenario. This distinction arose because the Singlino component predominantly contributed to the DM candidate for nearly all samples in the h_1 scenario, necessitating a non-zero κ to account for the observed relic abundance. In contrast, in the h_2 scenario, a significant portion of samples featured Bino-dominated DM, whose properties were less influenced by κ .
- For both the h_1 and h_2 scenarios, $\tan \beta$ spanned a broad range from 5 to 60. The distributions did not show a significant preference for specific regions, suggesting that the DM physics are not sensitive to $\tan \beta$.

- The PL distributions suggest that μ_{tot} can range from 100 GeV to 1 TeV in both scenarios. However, μ_{tot} 's posterior PDF distributions indicated a preference for smaller μ_{tot} in the h_2 scenario. This preference was driven by the constraints from the Higgs data fit, which limited $\lambda\mu_{\text{tot}}$ in $\mathcal{M}_{\text{S},23}^2$ to be no more than approximately 30 GeV, a restriction not applicable to the h_1 scenario.
- Similarly, a relatively light DM was favored in the h_2 scenario, stemming from the condition $|m_{\tilde{\chi}_1^0}| < \mu_{\text{tot}}$ and the observed preference for a smaller μ_{tot} in this scenario. Additionally, a light DM is self-consistent with the annihilation $\tilde{\chi}_1^0 \tilde{\chi}_1^0 \rightarrow h_s h_s$, where h_s could be as light as several GeV in the h_2 scenario.

We also investigated the impact of the LHC search for supersymmetry on the distributions. In the h_1 scenario, we observed that it only shifted the lower bounds of $m_{\tilde{\chi}_1^0}$ and μ_{tot} in the PL distribution from 34 and 105 GeV to approximately 48 and 165 GeV, respectively. In contrast, in the h_2 scenario, apart from altering the lower bounds on $m_{\tilde{\chi}_1^0}$ and μ_{tot} from 14 and 100 GeV to approximately 40 and 155 GeV, respectively, the LHC constraint significantly modified their posterior PDFs by shifting the peaks of their distribution toward higher mass values. The updated results are shown in Fig. 3 compared to their corresponding ones in Fig. 2. This phenomenon arose due to the crucial nature of the LHC constraints when the DM and Higgsinos had moderately low masses. This effect was less pronounced on other distributions of the h_2 scenario.

Finally, we projected the samples passing the LHC constraint onto the $|m_{\tilde{\chi}_1^0}| - \sigma_{\tilde{\chi}_1^0-p}^{\text{SI}}$ and $|m_{\tilde{\chi}_1^0}| - \sigma_{\tilde{\chi}_1^0-n}^{\text{SD}}$ planes to obtain two-dimensional posterior PDF maps, which are shown in Fig. 4. This figure reveals that the samples in the 2σ credible region predicted $1.0 \times 10^{-49} \lesssim \sigma_{\tilde{\chi}_1^0-p}^{\text{SI}}/\text{cm}^2 \lesssim 2.5 \times 10^{-46}$ and $1.0 \times 10^{-50} \lesssim \sigma_{\tilde{\chi}_1^0-n}^{\text{SD}}/\text{cm}^2 \lesssim 3.2 \times 10^{-43}$ in the h_1 scenario. In contrast, analyzing the h_2 scenario yielded $5.0 \times 10^{-49} \lesssim \sigma_{\tilde{\chi}_1^0-p}^{\text{SI}}/\text{cm}^2 \lesssim 2.0 \times 10^{-46}$ and $1.0 \times 10^{-52} \lesssim \sigma_{\tilde{\chi}_1^0-n}^{\text{SD}}/\text{cm}^2 \lesssim 1.0 \times 10^{-43}$ for Singlino-like DM and $3.0 \times 10^{-49} \lesssim \sigma_{\tilde{\chi}_1^0-p}^{\text{SI}}/\text{cm}^2 \lesssim 2.0 \times 10^{-46}$, $1.0 \times 10^{-43} \lesssim \sigma_{\tilde{\chi}_1^0-n}^{\text{SD}}/\text{cm}^2 \lesssim 5.0 \times 10^{-42}$ for Bino-like DM. These results showed significant difference of $\sigma_{\tilde{\chi}_1^0-n}^{\text{SD}}$ for Singlino- and Bino-like DM, which was explained in Eqs. (2.41) and (2.42). Additionally, they revealed that with the future increase in experimental sensitivities to $\sigma_{\tilde{\chi}_1^0-p}^{\text{SI}}$, a significant portion of the samples would become disfavored. Numerically speaking, we observed that the Bayesian evidences decreased by 46% and 62% for the h_1 and h_2 scenarios, respectively, if the sensitivities were improved by a factor of 5. Consequently, the upper bounds of λ were reduced to approximately 0.05 and 0.02, respectively.

3.3 Three annihilation channels

As introduced in Section 2.3, the relic abundance and nucleon scattering cross sections of the Singlino-dominated DM depend not only on parameters within the neu-

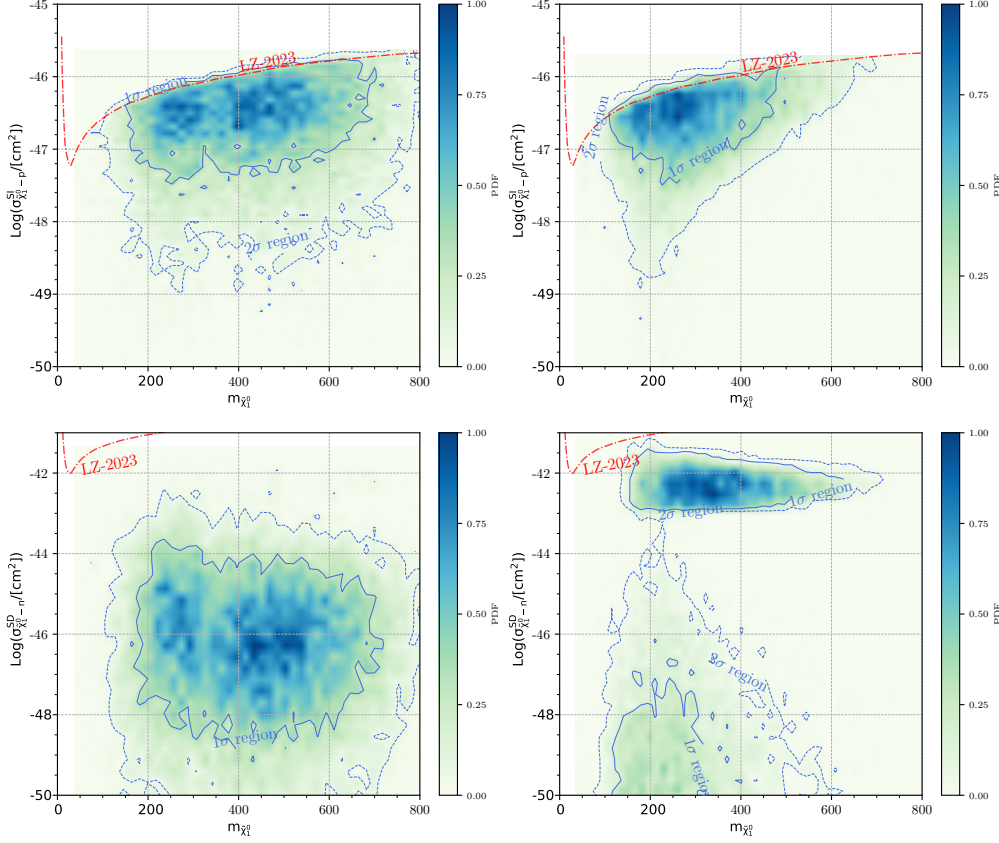


Figure 4. Two-dimensional distributions of the marginal posterior PDF for the likelihood \mathcal{L} in Eq. 3.3, projected onto the $|m_{\tilde{\chi}_1^0}| - \sigma_{\tilde{\chi}_1^0-p}^{SI}$ and $|m_{\tilde{\chi}_1^0}| - \sigma_{\tilde{\chi}_1^0-n}^{SD}$ planes. The left panels show the results of the h_1 scenario, while the right panels show those of the h_2 scenario. The solid and dashed lines surround the 1σ and 2σ credible regions, respectively, and the samples falling within these regions contributed 65.3% and 95.4% of the total Bayesian evidence [95]. All the considered samples were consistent with the LHC constraint.

tralino sector, including λ , κ , $\tan \beta$, μ_{tot} , and $m_{\tilde{\chi}_1^0}$, but also on those within the Higgs sector, such as v_s , A_λ , m_B (or equivalently m_{h_s}), and m_C (m_{A_s}). Consequently, the characteristics of the DM are complex. Nevertheless, valuable insights can still be obtained from scattering plots derived from our sample sets. We categorized the samples based on their predominant annihilation processes for this study's purposes. We particularly focus on samples where the primary annihilation mechanisms were $\tilde{\chi}_1^0 \tilde{\chi}_1^0 \rightarrow h_s h_s$, $\tilde{\chi}_1^0 \tilde{\chi}_1^0 \rightarrow A_s A_s$, and $\tilde{\chi}_1^0 \tilde{\chi}_1^0 \rightarrow h_s A_s$, and label them as Type-I, Type-II, and Type-III samples, respectively. Their respective counts were approximately 8000, 8000, and 16000 samples obtained by the scans, which created a challenge in plot representations and complicated our analyses due to their sheer volume. To address this issue, we applied a method introduced in Ref. [19] to reduce the sample density for the first two types of samples, while for the latter type, we controlled its sample size by implementing a mass constraint of $0.8m_{h_s} \lesssim m_{A_s} \lesssim 1.2m_{h_s}$ to simplify our analysis. By comparing plots derived from the full sample sets with

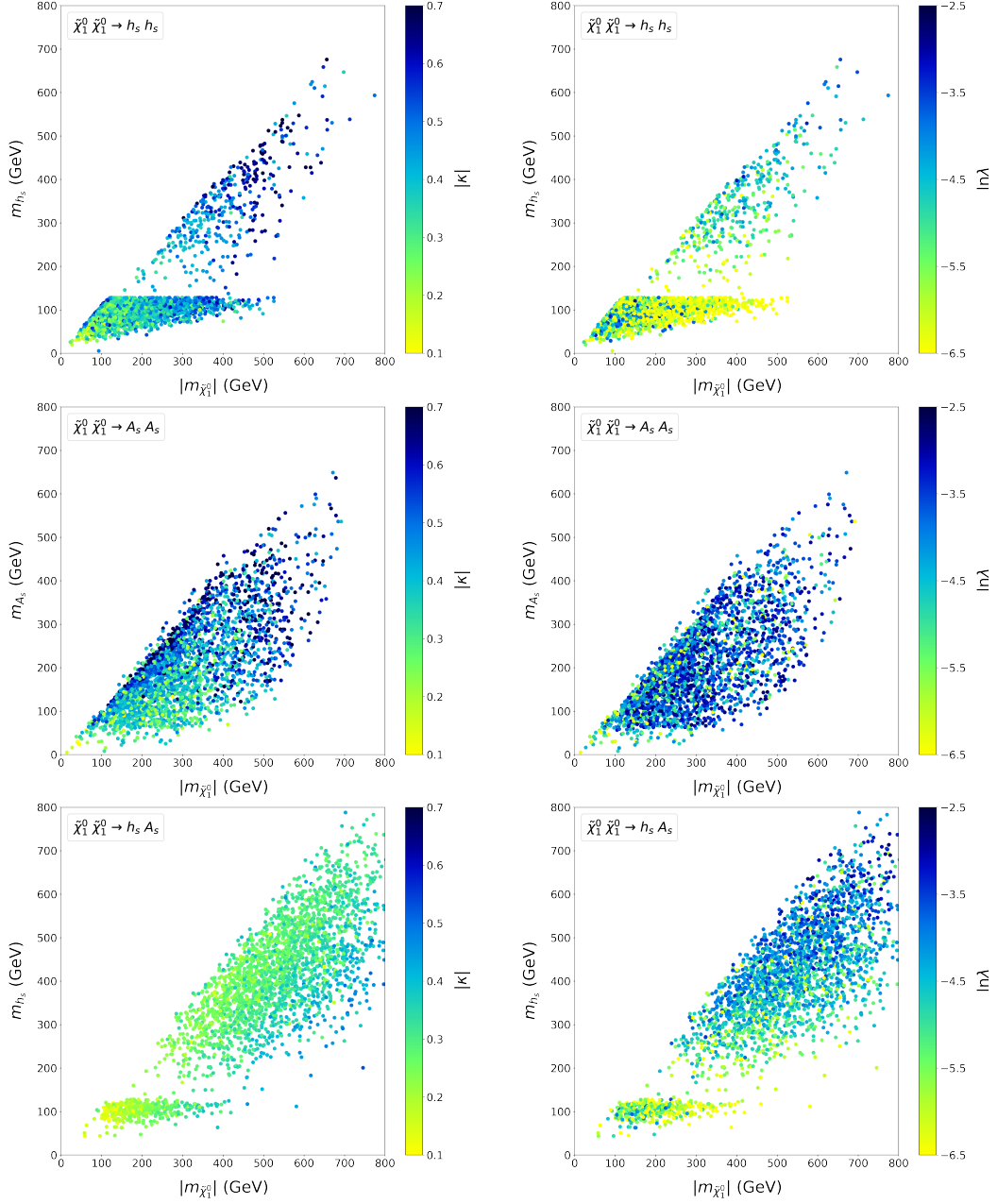


Figure 5. Scattering plots of the samples that primarily annihilated through $\tilde{\chi}_1^0 \tilde{\chi}_1^0 \rightarrow h_s h_s, A_s A_s, h_s A_s$ channels to achieve the observed relic abundance, projected onto the $|m_{\tilde{\chi}_1^0}| - m_{h_s}$, $|m_{\tilde{\chi}_1^0}| - m_{A_s}$, and $|m_{\tilde{\chi}_1^0}| - m_{h_s}$ planes, respectively. The color bars on the left panels denote the values of $|\kappa|$, while those on the right panels represent the values of $\ln \lambda$.

those from the reduced sample sets, we observed that the latter efficiently captured essential features of the annihilations without losing the generality of our findings.

In Fig. 5, we project three types of samples onto the $|m_{\tilde{\chi}_1^0}| - m_{h_s}$, $|m_{\tilde{\chi}_1^0}| - m_{A_s}$,

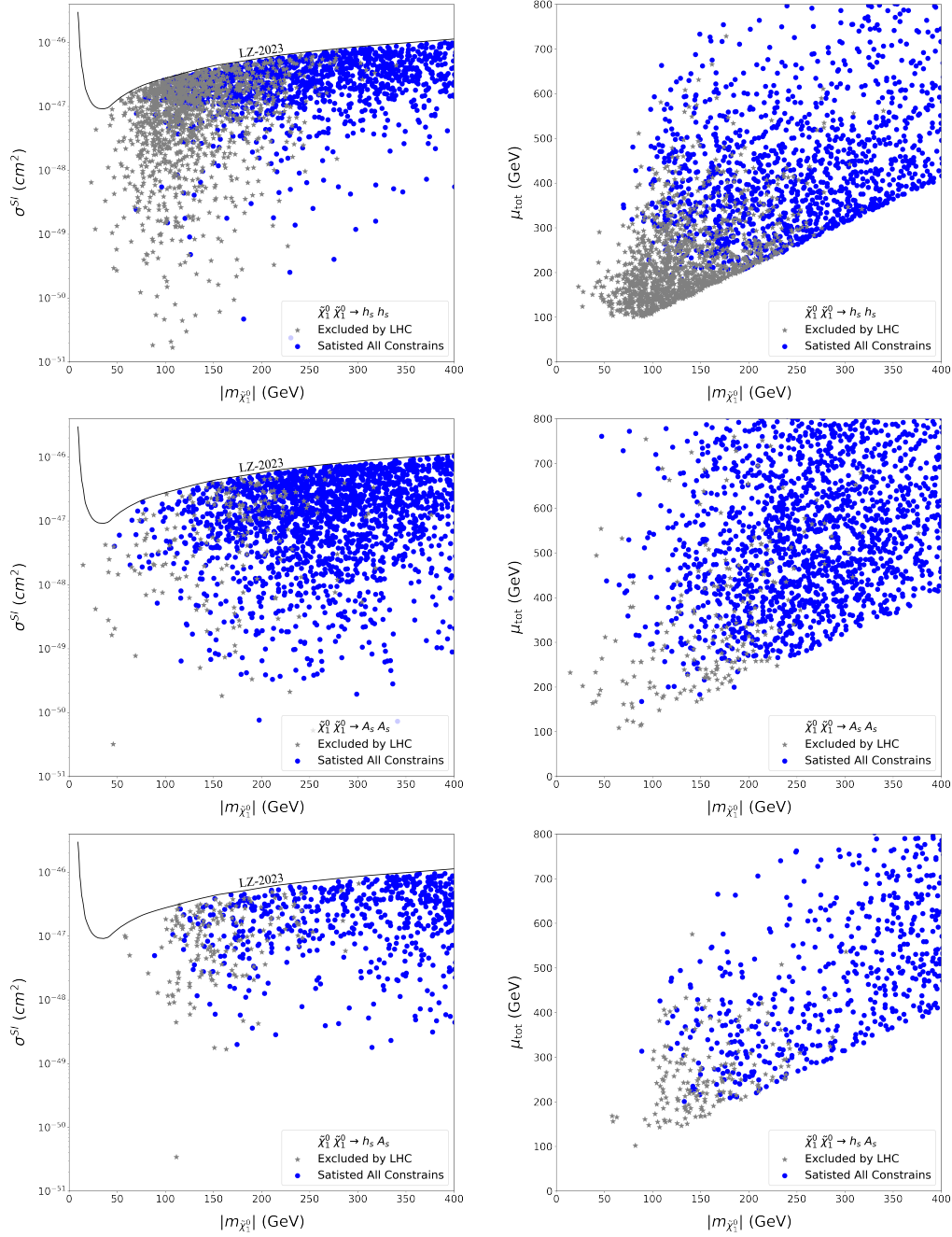


Figure 6. Similar to Fig. 5, except that the results are shown on the $|m_{\tilde{\chi}_1^0}| - \sigma_{\tilde{\chi}_1^0-p}^{\text{SI}}$ (left panels) and $|m_{\tilde{\chi}_1^0}| - \mu_{\text{tot}}$ (right panels) planes. Samples marked by gray were excluded by the LHC constraint, while those in blue were consistent with all the experimental constraints.

and $|m_{\tilde{\chi}_1^0}| - m_{h_s}$ planes, respectively. The color bar on the left panels indicates the value of $|\kappa|$, which is crucial in determining the relic abundance. On the right panel, the color bar shows the value of $\ln \lambda$, critical for DM-nucleon scattering cross sections.

Point P1				Point P2			
λ	0.012	m_{h_s}	269.8 GeV	λ	0.003	m_{h_s}	119.3 GeV
κ	-0.40	m_h	125.6 GeV	κ	0.56	m_h	124.9 GeV
$\tan \beta$	16.58	m_H	1826 GeV	$\tan \beta$	11.75	m_H	1871 GeV
v_s	692.3 GeV	m_{A_s}	737.5 GeV	v_s	609.2 GeV	m_{A_s}	735.6 GeV
μ_{tot}	390.4 GeV	m_{A_H}	1826 GeV	μ_{tot}	405.2 GeV	m_{A_H}	1871 GeV
M_1	-747.5 GeV	m_{H^\pm}	1827 GeV	M_1	-718.8 GeV	m_{H^\pm}	1872 GeV
M_2	822.5 GeV	$m_{\tilde{\chi}_1^0}$	324.2 GeV	M_2	614.6 GeV	$m_{\tilde{\chi}_1^0}$	339 GeV
A_t	-3983 GeV	$m_{\tilde{\chi}_2^0}$	393.2 GeV	A_t	-4233 GeV	$m_{\tilde{\chi}_2^0}$	400.5 GeV
A_λ	1654 GeV	$m_{\tilde{\chi}_3^0}$	-400 GeV	A_λ	1562 GeV	$m_{\tilde{\chi}_3^0}$	-414.6 GeV
m_A	2000 GeV	$m_{\tilde{\chi}_4^0}$	-755.3 GeV	m_A	2000 GeV	$m_{\tilde{\chi}_4^0}$	660.3 GeV
m_B	280.8 GeV	$m_{\tilde{\chi}_5^0}$	865.1 GeV	m_B	109.5 GeV	$m_{\tilde{\chi}_5^0}$	-726.7 GeV
m_N	326.3 GeV	$m_{\tilde{\chi}_1^\pm}$	395 GeV	m_N	345.1 GeV	$m_{\tilde{\chi}_1^\pm}$	402.5 GeV
Ωh^2	0.1199	$m_{\tilde{\chi}_2^\pm}$	865.3 GeV	Ωh^2	0.12	$m_{\tilde{\chi}_2^\pm}$	660.6 GeV
$\sigma_{\tilde{\chi}_1^0\tilde{\chi}_1^0 \rightarrow h_s h_s}^{\text{SD}}$	$1.73 \times 10^{-46} \text{ cm}^2$	$\sigma_{\tilde{\chi}_1^0\tilde{\chi}_1^0 \rightarrow p\bar{p}}^{\text{SI}}$	$2.24 \times 10^{-47} \text{ cm}^2$	$\sigma_{\tilde{\chi}_1^0\tilde{\chi}_1^0 \rightarrow h_s h_s}^{\text{SD}}$	$7.42 \times 10^{-49} \text{ cm}^2$	$\sigma_{\tilde{\chi}_1^0\tilde{\chi}_1^0 \rightarrow p\bar{p}}^{\text{SI}}$	$7.19 \times 10^{-47} \text{ cm}^2$
$V_{h_s}^{\text{S}}, V_{h_s}^{\text{SM}}, V_h^{\text{S}}, V_h^{\text{SM}}$	-0.999, -0.019, 0.019, -0.999			$V_{h_s}^{\text{S}}, V_{h_s}^{\text{SM}}, V_h^{\text{S}}, V_h^{\text{SM}}$	0.982, -0.190, 0.190, 0.982		
$N_{11}, N_{12}, N_{13}, N_{14}, N_{15}$	0.001, 0.002, -0.012, 0.015, -0.999			$N_{11}, N_{12}, N_{13}, N_{14}, N_{15}$	0.001, 0.001, -0.003, 0.004, -0.999		
$N_{21}, N_{22}, N_{23}, N_{24}, N_{25}$	-0.028, -0.126, 0.706, -0.696, -0.020			$N_{21}, N_{22}, N_{23}, N_{24}, N_{25}$	-0.028, -0.239, 0.696, -0.676, -0.005		
$N_{31}, N_{32}, N_{33}, N_{34}, N_{35}$	-0.081, -0.042, -0.704, -0.704, -0.002			$N_{31}, N_{32}, N_{33}, N_{34}, N_{35}$	-0.090, -0.048, -0.703, -0.704, -0.001		
$N_{41}, N_{42}, N_{43}, N_{44}, N_{45}$	0.996, -0.004, -0.037, -0.078, -0.001			$N_{41}, N_{42}, N_{43}, N_{44}, N_{45}$	0.007, -0.970, -0.136, 0.202, 0.001		
$N_{51}, N_{52}, N_{53}, N_{54}, N_{55}$	0.003, -0.991, -0.060, 0.118, 0.001			$N_{51}, N_{52}, N_{53}, N_{54}, N_{55}$	0.996, -0.005, -0.043, -0.084, -0.001		
annihilations	Fractions [%]			annihilations	Fractions [%]		
$\tilde{\chi}_1^0\tilde{\chi}_1^0 \rightarrow h_s h_s$	99.9			$\tilde{\chi}_1^0\tilde{\chi}_1^0 \rightarrow h_s h_s / h_s h$	92.7/7.02		
Decays	Branching ratios [%]			Decays	Branching ratios [%]		
$\tilde{\chi}_2^0 \rightarrow \tilde{\chi}_1^0 Z^*$	100			$\tilde{\chi}_2^0 \rightarrow \tilde{\chi}_1^0 Z^*$	100		
$\tilde{\chi}_3^0 \rightarrow \tilde{\chi}_1^0 Z^*$	96.5			$\tilde{\chi}_3^0 \rightarrow \tilde{\chi}_1^0 (W^\pm)^* / \tilde{\chi}_2^0 Z^* / \tilde{\chi}_1^0 Z^*$	51.8/40.7/8.5		
$\tilde{\chi}_4^0 \rightarrow \tilde{\chi}_1^\pm W^\mp / \tilde{\chi}_3^0 h / \tilde{\chi}_2^0 Z / \tilde{\chi}_3^0 Z$	50/22.5/21.5/3			$\tilde{\chi}_4^0 \rightarrow \tilde{\chi}_1^\pm W^\mp / \tilde{\chi}_3^0 Z / \tilde{\chi}_2^0 h$	55.8/22.5/19.2		
$\tilde{\chi}_5^0 \rightarrow \tilde{\chi}_1^\pm W^\mp / \tilde{\chi}_3^0 Z / \tilde{\chi}_2^0 h$	51.7/22.2/21			$\tilde{\chi}_5^0 \rightarrow \tilde{\chi}_1^\pm W^\mp / \tilde{\chi}_3^0 h / \tilde{\chi}_2^0 Z$	50.4/21.8/21.6		
$\tilde{\chi}_1^\pm \rightarrow \tilde{\chi}_1^0 (W^\pm)^*$	100			$\tilde{\chi}_1^\pm \rightarrow \tilde{\chi}_1^0 (W^\pm)^*$	100		
$\tilde{\chi}_2^\pm \rightarrow \tilde{\chi}_3^0 W^\pm / \tilde{\chi}_3^0 W^\pm / \tilde{\chi}_2^\pm Z / \tilde{\chi}_1^\pm h$	25.4/25.4/25.1/23.7			$\tilde{\chi}_2^\pm \rightarrow \tilde{\chi}_3^0 W^\pm / \tilde{\chi}_1^\pm Z / \tilde{\chi}_3^0 W^\pm / \tilde{\chi}_1^\pm h$	27.3/25.8/25.6/20.5		
$h_s \rightarrow W^+ W^- / Z Z / h h b$	56.4/23/20.4			$h_s \rightarrow b\bar{b} / WW^* / gg / \tau^+ \tau^-$	62.9/16.2/9.1/7.2		
$h \rightarrow b\bar{b} / WW^* / gg / \tau^+ \tau^-$	53.7/26.6/8.2/6.2			$h \rightarrow b\bar{b} / WW^* / gg / \tau^+ \tau^- / c\bar{c}$	54.9/25.2/8.3/6.4/2.5		
$H \rightarrow b\bar{b} / \tilde{\chi}_1^\pm \tilde{\chi}_2^\mp / \tilde{\chi}_3^0 \tilde{\chi}_5^0 / \tilde{\chi}_2^0 \tilde{\chi}_5^0 / \tau^+ \tau^-$	49.3/26.2/13.7/6/4.9			$H \rightarrow b\bar{b} / \tilde{\chi}_1^\pm \tilde{\chi}_2^\mp / \tilde{\chi}_3^0 \tilde{\chi}_4^0 / \tilde{\chi}_2^0 \tilde{\chi}_4^0 / \tilde{\chi}_1^\pm \tilde{\chi}_1^\mp$	46.6/15.9/12.4/7/3.7		
$A_H \rightarrow b\bar{b} / \tilde{\chi}_1^\pm \tilde{\chi}_2^\mp / \tilde{\chi}_3^0 \tilde{\chi}_5^0$	38.5/26.3/13.5			$A_H \rightarrow b\bar{b} / \tilde{\chi}_1^\pm \tilde{\chi}_2^\mp / \tilde{\chi}_3^0 \tilde{\chi}_4^0 / \tilde{\chi}_1^\pm \tilde{\chi}_1^\mp / \tilde{\chi}_2^0 \tilde{\chi}_5^0$	42.9/14.1/12.4/5.8/2.9		
$H^\pm \rightarrow t\bar{b} / \tilde{\chi}_1^0 \tilde{\chi}_2^\pm / \tilde{\chi}_3^0 \tilde{\chi}_4^\pm / \tilde{\chi}_3^0 \tilde{\chi}_2^\pm / \tilde{\chi}_4^0 \tilde{\chi}_1^\pm$	27.2/20.3/19.7/19.3/6.8			$H^\pm \rightarrow \tilde{\chi}_1^0 \tilde{\chi}_2^\pm / \tilde{\chi}_3^0 \tilde{\chi}_4^\pm / \tilde{\chi}_3^0 \tilde{\chi}_2^\pm / t\bar{b} / \tilde{\chi}_5^0 \tilde{\chi}_1^\pm$	25.9/24.4/22.9/14.8/6.3		
R value: 0.16	Signal Region: SR-incWh-SFOS-09 in Ref. [124]			R value: 0.33	Signal Region: SR-G05 in Ref. [126]		

Table 6. Benchmark points where the Singlino-dominated DM achieved the observed relic abundance primarily through the process $\tilde{\chi}_1^0\tilde{\chi}_1^0 \rightarrow h_s h_s$. Both points satisfied all experimental constraints. In the left and right parts of this table, h_1 and h_2 were predicted to be the SM-like Higgs boson, respectively.

Analysis of the left panels yielded the following conclusions:

- Increasing m_{h_s} in annihilation processes $\tilde{\chi}_1^0\tilde{\chi}_1^0 \rightarrow h_s h_s$ and $\tilde{\chi}_1^0\tilde{\chi}_1^0 \rightarrow h_s A_s$ or increasing m_{A_s} in annihilation process $\tilde{\chi}_1^0\tilde{\chi}_1^0 \rightarrow A_s A_s$ favors a larger $|\kappa|$ to reach the observed relic abundance at a fixed $|m_{\tilde{\chi}_1^0}|$. In particular, $|\kappa|$ reaches its maximum when the scalar mass closely matches the DM mass due to the phase space suppression in these annihilations.
- An increase in $|m_{\tilde{\chi}_1^0}|$ correlates with a preference for a higher $|\kappa|$ to achieve the observed relic abundance, which is demonstrated by the approximations in Eqs. (2.26), (2.29), and (2.32) for simplified cases.
- Among the three annihilations, $\tilde{\chi}_1^0\tilde{\chi}_1^0 \rightarrow h_s A_s$ requires the smallest $|\kappa|$ to achieve the observed relic abundance due to its s-wave nature, in contrast with the p-wave nature of the other channels. The comparison of $\tilde{\chi}_1^0\tilde{\chi}_1^0 \rightarrow A_s A_s$ with $\tilde{\chi}_1^0\tilde{\chi}_1^0 \rightarrow h_s h_s$ shows that the former prefers a larger $|\kappa|$, as explained by Eqs. (2.26) and (2.29).

Point P3				Point P4			
λ	0.006	m_{h_s}	818.5 GeV	λ	0.002	m_{h_s}	98.97 GeV
κ	0.45	m_h	124.7 GeV	κ	0.13	m_h	125.6 GeV
$\tan \beta$	26.64	m_H	1670 GeV	$\tan \beta$	25.25	m_H	1730 GeV
v_s	886.7 GeV	m_{A_s}	119.5 GeV	v_s	285.8 GeV	m_{A_s}	50.57 GeV
μ_{tot}	569 GeV	m_{A_H}	1670 GeV	μ_{tot}	428.2 GeV	m_{A_H}	1730 GeV
M_1	692.6 GeV	m_{H^\pm}	1665 GeV	M_1	732.2 GeV	m_{H^\pm}	1728 GeV
M_2	303.9 GeV	$m_{\tilde{\chi}_1^0}$	217.5 GeV	M_2	656.5 GeV	$m_{\tilde{\chi}_1^0}$	-65.31 GeV
A_t	-2748 GeV	$m_{\tilde{\chi}_2^0}$	314.8 GeV	A_t	-3168 GeV	$m_{\tilde{\chi}_2^0}$	422.4 GeV
A_λ	-1307 GeV	$m_{\tilde{\chi}_3^0}$	583.5 GeV	A_λ	-731.2 GeV	$m_{\tilde{\chi}_3^0}$	-441.9 GeV
m_A	2000 GeV	$m_{\tilde{\chi}_4^0}$	-584.1 GeV	m_A	2000 GeV	$m_{\tilde{\chi}_4^0}$	699.8 GeV
m_B	834.7 GeV	$m_{\tilde{\chi}_5^0}$	706.1 GeV	m_B	101 GeV	$m_{\tilde{\chi}_5^0}$	742 GeV
m_N	217.5 GeV	$m_{\tilde{\chi}_1^\pm}$	315.2 GeV	m_N	-65.37 GeV	$m_{\tilde{\chi}_1^\pm}$	428.5 GeV
Ωh^2	0.12	$m_{\tilde{\chi}_2^\pm}$	596.2 GeV	Ωh^2	0.1119	$m_{\tilde{\chi}_2^\pm}$	701.9 GeV
$\sigma_{\tilde{\chi}_1^0\text{-p}}^{\text{SD}}$	$5.37 \times 10^{-49} \text{ cm}^2$	$\sigma_{\tilde{\chi}_1^0\text{-p}}^{\text{SI}}$	$7.86 \times 10^{-49} \text{ cm}^2$	$\sigma_{\tilde{\chi}_1^0\text{-p}}^{\text{SD}}$	$6.11 \times 10^{-51} \text{ cm}^2$	$\sigma_{\tilde{\chi}_1^0\text{-p}}^{\text{SI}}$	$1.03 \times 10^{-47} \text{ cm}^2$
$V_{h_s}^{\text{S}}, V_{h_s}^{\text{SM}}, V_h^{\text{S}}, V_h^{\text{SM}}$	0.999, 0.002, -0.002, 0.999	$V_{h_s}^{\text{S}}, V_{h_s}^{\text{SM}}, V_h^{\text{S}}, V_h^{\text{SM}}$	-0.999, 0.043, -0.043, -0.999				
$N_{11}, N_{12}, N_{13}, N_{14}, N_{15}$	0.001, -0.002, 0.001, -0.002, 0.999	$N_{11}, N_{12}, N_{13}, N_{14}, N_{15}$	-0.001, 0.001, 0.001, 0.001, -0.999				
$N_{21}, N_{22}, N_{23}, N_{24}, N_{25}$	0.013, -0.975, 0.192, -0.108, -0.002	$N_{21}, N_{22}, N_{23}, N_{24}, N_{25}$	0.098, -0.212, 0.699, -0.676, -0.001				
$N_{31}, N_{32}, N_{33}, N_{34}, N_{35}$	0.264, 0.208, 0.664, -0.668, -0.002	$N_{31}, N_{32}, N_{33}, N_{34}, N_{35}$	-0.025, 0.048, 0.703, 0.709, 0.001				
$N_{41}, N_{42}, N_{43}, N_{44}, N_{45}$	-0.023, 0.059, 0.703, 0.708, 0.001	$N_{41}, N_{42}, N_{43}, N_{44}, N_{45}$	0.173, 0.965, 0.108, -0.166, -0.001				
$N_{51}, N_{52}, N_{53}, N_{54}, N_{55}$	0.964, -0.042, -0.167, 0.201, 0.001	$N_{51}, N_{52}, N_{53}, N_{54}, N_{55}$	0.980, -0.148, -0.071, 0.115, 0.001				
annihilations	Fractions [%]	annihilations	Fractions [%]				
$\tilde{\chi}_1^0 \tilde{\chi}_1^0 \rightarrow A_s A_s$	99.8	$\tilde{\chi}_1^0 \tilde{\chi}_1^0 \rightarrow A_s A_s$	99.9				
Decays	Branching ratios [%]	Decays	Branching ratios [%]				
$\tilde{\chi}_2^0 \rightarrow \tilde{\chi}_1^0 Z$	100	$\tilde{\chi}_2^0 \rightarrow \tilde{\chi}_1^0 Z / \tilde{\chi}_1^0 h$	62.2/37.2				
$\tilde{\chi}_3^0 \rightarrow \tilde{\chi}_1^\pm W^\mp / \tilde{\chi}_2^0 h / \tilde{\chi}_2^0 Z$	69.5/27.7/2.8	$\tilde{\chi}_3^0 \rightarrow \tilde{\chi}_1^0 h / \tilde{\chi}_2^0 Z / \tilde{\chi}_2^0 Z^* / \tilde{\chi}_1^\mp (W^\pm)^*$	45.3/29.5/14.6/5.8				
$\tilde{\chi}_4^0 \rightarrow \tilde{\chi}_1^\pm W^\mp / \tilde{\chi}_2^0 Z / \tilde{\chi}_2^0 h$	67.8/30.1/1.7	$\tilde{\chi}_4^0 \rightarrow \tilde{\chi}_1^\pm W^\mp / \tilde{\chi}_3^0 Z / \tilde{\chi}_2^0 h$	65.1/17.7/15.5				
$\tilde{\chi}_5^0 \rightarrow \tilde{\chi}_2^\pm W^\mp / \tilde{\chi}_1^\pm W^\mp / \tilde{\chi}_3^0 Z / \tilde{\chi}_2^0 Z$	37.1/29.7/19.4/1.8	$\tilde{\chi}_5^0 \rightarrow \tilde{\chi}_3^0 Z / \tilde{\chi}_3^0 h / \tilde{\chi}_2^\pm W^\mp$	38.4/34.8/22.2				
$\tilde{\chi}_1^\pm \rightarrow \tilde{\chi}_1^0 W^\pm$	100	$\tilde{\chi}_1^\pm \rightarrow \tilde{\chi}_1^0 W^\pm$	100				
$\tilde{\chi}_2^\pm \rightarrow \tilde{\chi}_2^0 W^\pm / \tilde{\chi}_1^\pm Z / \tilde{\chi}_1^\pm h$	35.6/34.5/29.9	$\tilde{\chi}_2^\pm \rightarrow \tilde{\chi}_2^0 W^\pm / \tilde{\chi}_1^\pm Z / \tilde{\chi}_3^0 W^\pm / \tilde{\chi}_1^\pm h$	26.4/26/25.4/22.1				
$h_s \rightarrow A_s A_s / \tilde{\chi}_1^0 \tilde{\chi}_1^0$	84.4/15.6	$h_s \rightarrow b\bar{b} / \tau^+ \tau^- / gg / c\bar{c}$	79.6/8.9/7.2/3.4				
$h \rightarrow b\bar{b} / WW^* / gg / \tau^+ \tau^-$	55.1/24.9/8.4/6.4	$h \rightarrow b\bar{b} / A_s A_s / WW^* / gg / \tau^+ \tau^-$	39.3/26.6/19.6/6.1/4.6				
$H \rightarrow b\bar{b} / \tilde{\chi}_1^\pm \tilde{\chi}_2^\mp / \tilde{\chi}_2^0 \tilde{\chi}_4^0 / \tau^+ \tau^- / \tilde{\chi}_5^0 \tilde{\chi}_5^0$	39.8/30/9.3/7.7/5.7	$H \rightarrow b\bar{b} / \tilde{\chi}_1^\pm \tilde{\chi}_2^\mp / \tilde{\chi}_3^0 \tilde{\chi}_4^0 \tau^+ \tau^- / \tilde{\chi}_3^0 \tilde{\chi}_5^0$	41.2/28.6/7.8/7.8/4.5				
$A_H \rightarrow b\bar{b} / \tilde{\chi}_1^\pm \tilde{\chi}_2^\mp / \tilde{\chi}_3^0 \tilde{\chi}_4^0 / \tau^+ \tau^- / \tilde{\chi}_2^0 \tilde{\chi}_4^0$	39.8/28.9/8.3/7.7/5.8	$A_H \rightarrow b\bar{b} / \tilde{\chi}_1^\pm \tilde{\chi}_2^\mp / \tau^+ \tau^- / \tilde{\chi}_2^0 \tilde{\chi}_4^0$	41.3/26.8/7.8/6.9				
$H^\pm \rightarrow t\bar{b} / \tilde{\chi}_3^0 \tilde{\chi}_1^\pm / \tilde{\chi}_3^0 \tilde{\chi}_2^\pm / \tilde{\chi}_4^0 \tilde{\chi}_1^\pm$	39.5/16.4/16.3/15.4	$H^\pm \rightarrow t\bar{b} / \tilde{\chi}_4^0 \tilde{\chi}_1^\pm / \tilde{\chi}_3^0 \tilde{\chi}_2^\pm / \tilde{\chi}_2^0 \tilde{\chi}_2^\pm / \tau^+ \nu_\tau$	41/17.6/14.2/15.3/8.6				
R value: 0.79	Signal Region: SR-incWZ-03 in Ref. [124]			R value: 0.85	Signal Region: SRG07-0j-mll in Ref. [126]		

Table 7. Same as Table 6 except that the Singlino-dominated DM achieved the observed relic abundance primarily through the process $\tilde{\chi}_1^0 \tilde{\chi}_1^0 \rightarrow A_s A_s$.

- The s-wave nature of the annihilation $\tilde{\chi}_1^0 \tilde{\chi}_1^0 \rightarrow h_s A_s$ with $h_s \rightarrow b\bar{b}$ and $A_s \rightarrow b\bar{b}$ also allows for indirect DM search experiments to establish a lower bound on $|m_{\tilde{\chi}_1^0}|$ (approximately 58 GeV). This bound is substantially less stringent than that of the direct annihilation $\tilde{\chi}_1^0 \tilde{\chi}_1^0 \rightarrow b\bar{b}$, as the power produced through the former channel is suppressed by its relatively heavy DM mass [144, 145]. In contrast, no experimental limits apply to p-wave annihilations $\tilde{\chi}_1^0 \tilde{\chi}_1^0 \rightarrow h_s h_s$ and $\tilde{\chi}_1^0 \tilde{\chi}_1^0 \rightarrow A_s A_s$, permitting potentially much lighter DM candidates down to 10 GeV.
- The complex dependence of the annihilation cross sections on the model's parameters suggests that all values of κ ranging from 0.05 to 0.75 are capable of providing an explanation for the observed relic abundance.

The information provided in the right panels is as follows:

- For Type-I and -III samples, λ is typically very small under the h_2 scenario due to significant singlet-doublet Higgs mixing, resulting in $\sigma_{\tilde{\chi}_1^0-\text{p}}^{\text{SI}}$ being proportional to $\lambda^2 \kappa^2$. Therefore, the results of the LZ experiment stringently limit the magnitude of λ . However, a significant λ may still be possible in rare cases where contributions mediated by h_s cancel out those mediated by h [47, 81].

Point P5				Point P6			
λ	0.026	m_{h_s}	462 GeV	λ	0.001	m_{h_s}	76.85 GeV
κ	-0.22	m_h	124.9 GeV	κ	0.18	m_h	125.2 GeV
$\tan \beta$	42.42	m_H	2389 GeV	$\tan \beta$	36.19	m_H	2148 GeV
v_s	630.1 GeV	m_{A_s}	263.4 GeV	v_s	200.7 GeV	m_{A_s}	282.8 GeV
μ_{tot}	514.5 GeV	m_{A_H}	2389 GeV	μ_{tot}	259 GeV	m_{A_H}	2148 GeV
M_1	855.2 GeV	m_{H^\pm}	2410 GeV	M_1	704.2 GeV	m_{H^\pm}	2159 GeV
M_2	822.6 GeV	$m_{\tilde{\chi}_1^0}$	-389.8 GeV	M_2	621.4 GeV	$m_{\tilde{\chi}_1^0}$	209.1 GeV
A_t	2492 GeV	$m_{\tilde{\chi}_2^0}$	515 GeV	A_t	2424 GeV	$m_{\tilde{\chi}_2^0}$	256.7 GeV
A_λ	1123 GeV	$m_{\tilde{\chi}_3^0}$	-529.8 GeV	A_λ	1501 GeV	$m_{\tilde{\chi}_3^0}$	-270.8 GeV
m_A	2000 GeV	$m_{\tilde{\chi}_4^0}$	858.4 GeV	m_A	2000 GeV	$m_{\tilde{\chi}_4^0}$	661.8 GeV
m_B	465.2 GeV	$m_{\tilde{\chi}_1^\pm}$	871.9 GeV	m_B	76.24 GeV	$m_{\tilde{\chi}_1^\pm}$	712.3 GeV
m_N	-390.2 GeV	$m_{\tilde{\chi}_2^\pm}$	520.2 GeV	m_N	209.5 GeV	$m_{\tilde{\chi}_2^\pm}$	262.1 GeV
Ωh^2	0.12	$m_{\tilde{\chi}_2^\pm}^{\text{SI}}$	867 GeV	Ωh^2	0.12	$m_{\tilde{\chi}_2^\pm}^{\text{SI}}$	662.9 GeV
$\sigma_{\tilde{\chi}_1^0 - p}^{\text{SD}}$	$8.24 \times 10^{-46} \text{ cm}^2$	$\sigma_{\tilde{\chi}_1^0 - p}^{\text{SI}}$	$1.9 \times 10^{-47} \text{ cm}^2$	$\sigma_{\tilde{\chi}_1^0 - p}^{\text{SD}}$	$9.89 \times 10^{-50} \text{ cm}^2$	$\sigma_{\tilde{\chi}_1^0 - p}^{\text{SI}}$	$3.76 \times 10^{-48} \text{ cm}^2$
$V_{h_s}^{\text{S}}, V_{h_s}^{\text{SM}}, V_h^{\text{S}}, V_h^{\text{SM}}$	0.999, 0.022, -0.022, 0.999	$V_{h_s}^{\text{S}}, V_{h_s}^{\text{SM}}, V_h^{\text{S}}, V_h^{\text{SM}}$	-0.999, 0.009, -0.009, -0.999				
$N_{11}, N_{12}, N_{13}, N_{14}, N_{15}$	0.001, -0.001, -0.014, -0.019, 0.999	$N_{11}, N_{12}, N_{13}, N_{14}, N_{15}$	-0.001, 0.001, -0.002, 0.002, -0.999				
$N_{21}, N_{22}, N_{23}, N_{24}, N_{25}$	-0.089, 0.163, -0.702, 0.687, 0.003	$N_{21}, N_{22}, N_{23}, N_{24}, N_{25}$	0.068, -0.141, 0.711, -0.685, -0.003				
$N_{31}, N_{32}, N_{33}, N_{34}, N_{35}$	0.022, -0.040, -0.704, -0.708, -0.023	$N_{31}, N_{32}, N_{33}, N_{34}, N_{35}$	0.031, -0.060, -0.700, -0.711, -0.001				
$N_{41}, N_{42}, N_{43}, N_{44}, N_{45}$	-0.564, -0.821, -0.046, 0.074, 0.001	$N_{41}, N_{42}, N_{43}, N_{44}, N_{45}$	0.112, 0.983, 0.056, -0.133, -0.001				
$N_{51}, N_{52}, N_{53}, N_{54}, N_{55}$	0.821, -0.545, -0.089, 0.145, 0.001	$N_{51}, N_{52}, N_{53}, N_{54}, N_{55}$	0.991, -0.099, -0.034, 0.085, 0.001				
annihilations	Fractions [%]	annihilations	Fractions [%]				
$\tilde{\chi}_1^0 \tilde{\chi}_1^0 \rightarrow h_s A_s$	99.6	$\tilde{\chi}_1^0 \tilde{\chi}_1^0 \rightarrow h_s A_s / h_s h_s$	97.1/2.87				
Decays	Branching ratios [%]	Decays	Branching ratios [%]				
$\tilde{\chi}_2^0 \rightarrow \tilde{\chi}_1^0 Z$	100	$\tilde{\chi}_2^0 \rightarrow \tilde{\chi}_1^0 Z^*$	100				
$\tilde{\chi}_3^0 \rightarrow \tilde{\chi}_1^0 h / \tilde{\chi}_1^0 Z$	92.5/7.38	$\tilde{\chi}_3^0 \rightarrow \tilde{\chi}_2^0 Z^* / \tilde{\chi}_1^\mp (W^\pm)^*$	79.5/20.4				
$\tilde{\chi}_4^0 \rightarrow \tilde{\chi}_1^\pm W^\mp / \tilde{\chi}_2^0 Z / \tilde{\chi}_3^0 h$	84.7/7.27/6.9	$\tilde{\chi}_4^0 \rightarrow \tilde{\chi}_1^\pm W^\mp / \tilde{\chi}_3^0 Z / \tilde{\chi}_2^0 h$	59.6/18.3/16				
$\tilde{\chi}_5^0 \rightarrow \tilde{\chi}_3^0 Z / \tilde{\chi}_2^0 h / \tilde{\chi}_2^0 Z / \tilde{\chi}_3^0 h$	47.9/45.1/3.12/2.39	$\tilde{\chi}_5^0 \rightarrow \tilde{\chi}_1^\pm W^\mp / \tilde{\chi}_3^0 Z / \tilde{\chi}_2^0 h / \tilde{\chi}_2^0 Z / \tilde{\chi}_3^0 h$	31.2/30.1/27.5/5.8/5.2				
$\tilde{\chi}_1^\pm \rightarrow \tilde{\chi}_1^0 (W^\pm)^*$	100	$\tilde{\chi}_1^\pm \rightarrow \tilde{\chi}_1^0 (W^\pm)^* / \tilde{\chi}_2^0 (W^\pm)^*$	53.2/46.8				
$\tilde{\chi}_2^\pm \rightarrow \tilde{\chi}_1^\pm Z / \tilde{\chi}_2^0 W^\pm / \tilde{\chi}_3^0 W^\pm / \tilde{\chi}_1^\pm h$	25.5/25.4/25.3/23.6	$\tilde{\chi}_2^\pm \rightarrow \tilde{\chi}_2^0 W^\pm / \tilde{\chi}_1^\pm Z / \tilde{\chi}_2^0 W^\pm / \tilde{\chi}_1^\pm h$	26/25.4/25/23.2				
$h_s \rightarrow W^+ W^- / hh / ZZ / b\bar{b}$	44.5/23/20/12.3	$h_s \rightarrow b\bar{b} / gg / \tau^+ \tau^-$	73/11/8				
$h \rightarrow b\bar{b} / WW^* / gg / \tau^+ \tau^- / c\bar{c}$	54.7/25.4/8.4/6.3/2.5	$h \rightarrow b\bar{b} / WW^* / gg / \tau^+ \tau^-$	54.2/25.9/8.4/6.3				
$H \rightarrow b\bar{b} / \tilde{\chi}_1^\pm \tilde{\chi}_2^\mp / \tau^+ \tau^- / \tilde{\chi}_3^0 \tilde{\chi}_5^0$	55.1/18.6/12.6/5.9	$H \rightarrow b\bar{b} / \tilde{\chi}_1^\pm \tilde{\chi}_2^\mp / \tau^+ \tau^- / \tilde{\chi}_3^0 \tilde{\chi}_4^0$	49.6/23.7/9.5/6				
$A_H \rightarrow b\bar{b} / \tilde{\chi}_1^\pm \tilde{\chi}_2^\mp / \tau^+ \tau^- / \tilde{\chi}_3^0 \tilde{\chi}_5^0$	55.1/18/12.6/5.5	$A_H \rightarrow b\bar{b} / \tilde{\chi}_1^\pm \tilde{\chi}_2^\mp / \tau^+ \tau^- / \tilde{\chi}_3^0 \tilde{\chi}_4^0$	49.6/23.5/9.5/5.7				
$H^\pm \rightarrow t\bar{b} / \tau^\pm \nu_\tau / \tilde{\chi}_1^0 \tilde{\chi}_2^\pm / \tilde{\chi}_3^0 \tilde{\chi}_2^\pm / \tilde{\chi}_3^0 \tilde{\chi}_2^\pm$	54.4/13.7/12.5/9.6/9.2	$H^\pm \rightarrow t\bar{b} / \tilde{\chi}_1^0 \tilde{\chi}_2^\pm / \tilde{\chi}_3^0 \tilde{\chi}_2^\pm / \tilde{\chi}_3^0 \tilde{\chi}_2^\pm$	49/13.5/12.5/11.7				
R value: 0.10	Signal Region: 3LI in Ref. [124]	R value: 0.74	Signal Region: SR-WZoff-high-njd in Ref. [126]				

Table 8. Same as Table 6 except that the Singlino-dominated DM achieved the observed relic abundance primarily through the process $\tilde{\chi}_1^0 \tilde{\chi}_1^0 \rightarrow h_s A_s$.

- As m_{h_s} and $|m_{\tilde{\chi}_1^0}|$ increase from 300 GeV for Type-I and -III samples, larger λ values may arise. In such instances, the singlet-doublet Higgs mixing is very small, resulting in the dominant contribution to $\sigma_{\tilde{\chi}_1^0 - p}^{\text{SI}}$ being proportional to λ^4 . Moreover, the contribution mediated by h_s is gradually reduced, and simultaneously, the LZ constraint is relaxed, both allowing for relatively large λ values, particularly when $\tilde{\chi}_1^0$ and h_s are all massive.
- In Type-II samples, the value of λ can significantly increase when the values of $|m_{\tilde{\chi}_1^0}|$ and m_{A_s} are enhanced from their starting point at $m_{\tilde{\chi}_1^0} \simeq 10$ GeV and $m_{A_s} \simeq 10$ GeV. Specifically, for this type of sample, h_s is always heavier than $\tilde{\chi}_1^0$, exceeding 300 GeV for almost all cases, which results in a minor impact on $\sigma_{\tilde{\chi}_1^0 - p}^{\text{SI}}$. The behavior of λ can be explained by two typical mass spectrum configurations: increasing $|m_{\tilde{\chi}_1^0}|$ while keeping m_{A_s} constant or fixing the ratio $m_{A_s}/|m_{\tilde{\chi}_1^0}|$ and increasing $|m_{\tilde{\chi}_1^0}|$. In both cases, the lower limit of m_{h_s} increases since $m_{h_s} > 2m_{\tilde{\chi}_1^0} - m_{A_s}$, leading to the tendency to decrease its contribution to $\sigma_{\tilde{\chi}_1^0 - p}^{\text{SI}}$. Along with the relaxation of the LZ constraint, this situation allows for larger values of λ .
- Compared to Type-I and -III samples, a larger portion of Type-II samples pre-

dict a sizable λ . The prevalence of large λ values in Type-II samples can be attributed to the tendency for a heavy h_s , resulting in the dominant contribution to $\sigma_{\tilde{\chi}_1^0-p}^{\text{SI}}$ being proportional to λ^4 . Additionally, Type-I samples favor smaller values of λ compared to Type-III samples largely due to a significant number of samples predicting relatively small μ_{tot} values.

We have also projected three types of samples onto the $|m_{\tilde{\chi}_1^0}| - \sigma_{\tilde{\chi}_1^0-p}^{\text{SI}}$ and $|m_{\tilde{\chi}_1^0}| - \mu_{\text{tot}}$ planes to create Fig. 6. In this visualization, gray indicates samples excluded by the LHC constraint, while blue represents samples in agreement with all experimental constraints. Fig. 6 reveals the following key observations:

- The LZ experiment and the LHC’s search for supersymmetry complement each other in restricting the parameter space of the GNMSSM.
- Type-II samples tend to predict a smaller $\sigma_{\tilde{\chi}_1^0-p}^{\text{SI}}$ than the other sample types.
- The LHC constraint is particularly effective in ruling out samples that predict moderately light DM and Higgsinos, notably enhancing lower limits on $|m_{\tilde{\chi}_1^0}|$ from approximately 23, 14, and 58 GeV to approximately 70, 47, and 89 GeV for Type-I, -II, and -III samples, respectively. Additionally, it set a lower bound of approximately 180 GeV on the Higgsino mass, which is much smaller than that of the MSSM [19].
- Among three types of samples, the Type-I samples are significantly more impacted by the LHC constraint due to its inclination toward moderately light Higgsinos.

In Tables 6, 7, and 8, we present benchmark points for three types of samples in both h_1 and h_2 scenarios. The detailed information of these points elucidate the underlying physics of Singlino-dominated DM.

4 Summary

Traditional supersymmetric models like the MSSM and \mathbb{Z}_3 -NMSSM are facing increasingly stringent constraints as direct detection experiments for DM and searches for supersymmetry at the LHC continue to advance rapidly. This has led to significant fine-tuning of the parameters within these models to predict viable DM candidates, as evidenced by Refs. [15, 31, 47]. In response to these challenges, we undertook Bayesian analyses of the GNMSSM to thoroughly explore its DM physics.

First, we examined the theoretical structure of the GNMSSM and selected a set of physical parameters as our input criteria. We constructed a comprehensive likelihood function that incorporated current experimental and theoretical knowledge on DM physics—including relic density and direct and indirect DM searches—as well

as Higgs and B physics. This likelihood function was then used to guide detailed scans of the theory’s parameter space using the nested sampling algorithm. We analyzed the resulting samples using statistical measures such as the PL and marginal posterior PDF to uncover underlying physical phenomena. Our findings indicated that the DM candidates in the GNMSSM may predominantly be either Singlino- or Bino-like DM. Specifically, the Singlino-like scenario accounted for 99.3% of the Bayesian evidence in the h_1 scenario and 64.8% in the h_2 scenario. Given that the Bayesian evidence significantly favored the h_1 scenario over the h_2 scenario, we concluded that the GNMSSM generally preferred Singlino-dominated DM across a much broader parameter range. This preference distinctly set the GNMSSM apart from the MSSM and \mathbb{Z}_3 -NMSSM, highlighting its unique position within the landscape of supersymmetric models.

Second, we examined the characteristics of Singlino-dominated DM and identified significant distinctions from the \mathbb{Z}_3 -NMSSM. In the latter, DM properties were determined by four parameters: λ , $\tan\beta$, μ_{eff} , and $m_{\tilde{\chi}_1^0} \simeq 2\kappa\mu_{\text{eff}}/\lambda$. For a Singlino-dominated neutralino to remain the LSP, $|\kappa|$ had to be smaller than $\lambda/2$. Furthermore, the LZ constraint on λ necessitated $|\kappa|$ to be very small. As a result, the Singlino DM in the \mathbb{Z}_3 -NMSSM needed to co-annihilate with electroweakinos to match the observed relic abundance. However, such dynamics differed in the GNMSSM due to the introduction of \mathbb{Z}_3 -violating terms where the DM’s properties were described through five independent parameters: λ , κ , $\tan\beta$, μ_{tot} , and $m_{\tilde{\chi}_1^0}$. Specifically, allowing for decorrelation of $m_{\tilde{\chi}_1^0}$ from μ_{tot} enables $|\kappa|$ to exceed λ when predicting Singlino-dominant DM. This structural difference significantly impacted the potential creation of a secluded DM sector within singlet particles [51]. The key characteristics of the secluded sector in our analysis included the following:

- Annihilation primarily occurred through the channels $\tilde{\chi}_1^0\tilde{\chi}_1^0 \rightarrow h_s h_s$, $\tilde{\chi}_1^0\tilde{\chi}_1^0 \rightarrow A_s A_s$, and $\tilde{\chi}_1^0\tilde{\chi}_1^0 \rightarrow h_s A_s$ to achieve the observed relic abundance. Among the parameters affecting the annihilation cross sections, κ played a crucial role, with $\tilde{\chi}_1^0\tilde{\chi}_1^0 \rightarrow h_s A_s$ preferring the smallest $|\kappa|$ value compared to other channels. However, due to the complex dependence of the annihilation cross sections on the model parameters, the values of $|\kappa|$ ranging from 0.05 to 0.75 were all capable of explaining the observed relic densities.
- The s-wave nature of $\tilde{\chi}_1^0\tilde{\chi}_1^0 \rightarrow h_s A_s$ resulted in a lower limit on $m_{\tilde{\chi}_1^0}$ at approximately 60 GeV from indirect DM search experiments, whereas in other channels, $m_{\tilde{\chi}_1^0}$ could decrease to as low as 10 GeV.
- The equations governing the interactions between DM and nucleons were characterized by parameters λ , κ , $\tan\beta$, μ_{tot} , and $m_{\tilde{\chi}_1^0}$, with λ exerting the most significant influence. It was observed that $\sigma_{\tilde{\chi}_1^0-p}^{\text{SI}}$ was proportional to $\lambda^2\kappa^2$ in the presence of substantial singlet–doublet Higgs mixing, and to λ^4 if h_s was very

massive. In contrast, $\sigma_{\tilde{\chi}_1^0-n}^{\text{SD}}$ consistently varied as a function of approximately λ^4 . Numerical analyses indicated that for most samples in the h_1 scenario, $\lambda \lesssim 0.09$; for the h_2 scenario, it was suggested that $\lambda \lesssim 0.05$. Consequently, $\sigma_{\tilde{\chi}_1^0-p}^{\text{SI}}$ and $\sigma_{\tilde{\chi}_1^0-n}^{\text{SD}}$ could be as low as 10^{-49} and 10^{-52} cm², respectively. Additionally, among the considered channels, $\tilde{\chi}_1^0\tilde{\chi}_1^0 \rightarrow h_s h_s$ in the h_2 scenario faced most stringent constraints from the LZ experiment due to the significant Higgs mixing and its preference for relatively light Higgsinos.

- For Singlino-like DM in the GNMSSM, although $\sigma_{\tilde{\chi}_1^0-p}^{\text{SI}}$ could approach the exclusion limits set by the LZ experiment, $\sigma_{\tilde{\chi}_1^0-n}^{\text{SD}}$ remained well below these bounds. Conversely, both $\sigma_{\tilde{\chi}_1^0-p}^{\text{SI}}$ and $\sigma_{\tilde{\chi}_1^0-n}^{\text{SD}}$ could reach exclusion limits for Bino-like DM. This observation suggested that if SD scattering were observed in near future, the viability of Singlino-like DM would be significantly undermined.
- In exceptional cases, Singlino-dominated DM could achieve observed relic abundance by co-annihilating with either Higgsino- (for most cases) or Wino-like electroweakinos, with permissible values for μ_{tot} down to approximate 200 GeV. In contrast, Bino-like DM with a mass at the electroweak scale could only co-annihilate with Wino-like electroweakinos to achieve correct abundance, and the LZ experiment set a threshold for μ_{tot} at approximately 380 GeV.

Finally, we investigated the impact of the LHC’s search for supersymmetry on DM physics, which was effective in excluding scenarios that predicted moderately light DM and Higgsinos. Our findings suggested that this constraint significantly raised the lower limits for $|m_{\tilde{\chi}_1^0}|$ from approximately 23, 14, and 58 GeV in $\tilde{\chi}_1^0\tilde{\chi}_1^0 \rightarrow h_s h_s$, $\tilde{\chi}_1^0\tilde{\chi}_1^0 \rightarrow A_s A_s$, and $\tilde{\chi}_1^0\tilde{\chi}_1^0 \rightarrow h_s A_s$ to about 70, 47, and 89 GeV, respectively. Moreover, a lower limit of around 180 GeV was imposed on the Higgsino mass, representing a significant departure from assumptions in the MSSM [19]. Notably, among these channels, $\tilde{\chi}_1^0\tilde{\chi}_1^0 \rightarrow h_s h_s$ was most influenced by the LHC constraint due to its preference for moderately light Higgsinos.

This study differed from our previous work cited in Ref. [49] in the following aspects.

- In contrast to Ref. [49], which focused on the μ -term-extended NMSSM and investigated the viability of Singlino-dominated DM, Bayesian analyses were conducted in this study within a general theoretical framework of the NMSSM. Specifically, we proposed a set of parameters with clear physical meanings as theoretical inputs and concluded that the theory favors Singlino-dominated DM across a much wider parameter space compared to Bino-like DM.
- We incorporated the most recent experimental results to constrain the DM physics of the GNMSSM, including the 2023 LZ search for both SI and SD

DM-nucleon scattering, various LHC searches for supersymmetry, and measurements of h 's couplings at the LHC with 136 fb^{-1} of data. We derived mass bounds on $\tilde{\chi}_1^0$ from indirect DM search experiments and the LHC supersymmetry search.

- We provide analytical formulas for the SI and SD cross sections of DM-nucleon scattering. These demonstrate that $\sigma_{\tilde{\chi}_1^0-p}^{\text{SI}}$ is proportional to $\lambda^2 \kappa^2$ amid substantial singlet-doublet Higgs mixing and λ^4 in heavy h_s limit, whereas $\sigma_{\tilde{\chi}_1^0-n}^{\text{SD}}$ consistently scales with λ^4 . Additionally, we present analytic expressions for the annihilation cross sections of $\tilde{\chi}_1^0 \tilde{\chi}_1^0 \rightarrow h_s h_s$, $\tilde{\chi}_1^0 \tilde{\chi}_1^0 \rightarrow A_s A_s$, and $\tilde{\chi}_1^0 \tilde{\chi}_1^0 \rightarrow h_s A_s$.

Our study delivered valuable insights into the DM physics of the GNMSSM, reopening the \mathbb{Z}_3 -NMSSM's extensive parameter space previously excluded by experiments. We eagerly anticipate further results from DM and LHC experiments that may provide more clues about the properties of DM and help pinpoint the correct theoretical framework.

Acknowledgments

J. Cao thanks Dr. Yuanfang Yue and Jinwei Lian for helpful discussions. This work was supported by the National Natural Science Foundation of China (NNSFC) under grant No. 12075076.

References

- [1] PLANCK collaboration, P. A. R. Ade et al., *Planck 2015 results. XIII. Cosmological parameters*, *Astron. Astrophys.* **594** (2016) A13 [[1502.01589](#)].
- [2] PLANCK collaboration, N. Aghanim et al., *Planck 2018 results. VI. Cosmological parameters*, *Astron. Astrophys.* **641** (2020) A6 [[1807.06209](#)].
- [3] K. Griest and M. Kamionkowski, *Supersymmetric dark matter*, *Phys. Rept.* **333** (2000) 167.
- [4] G. Bertone, D. Hooper and J. Silk, *Particle dark matter: Evidence, candidates and constraints*, *Phys. Rept.* **405** (2005) 279 [[hep-ph/0404175](#)].
- [5] S. Baum, M. Carena, N. R. Shah and C. E. M. Wagner, *Higgs portals for thermal Dark Matter. EFT perspectives and the NMSSM*, *JHEP* **04** (2018) 069 [[1712.09873](#)].
- [6] XENON collaboration, E. Aprile et al., *Dark Matter Search Results from a One Ton-Year Exposure of XENON1T*, *Phys. Rev. Lett.* **121** (2018) 111302 [[1805.12562](#)].
- [7] PANDAX-II collaboration, Q. Wang et al., *Results of dark matter search using the full PandaX-II exposure*, *Chin. Phys. C* **44** (2020) 125001 [[2007.15469](#)].

- [8] PANDAX-II collaboration, X. Cui et al., *Dark Matter Results From 54-Ton-Day Exposure of PandaX-II Experiment*, *Phys. Rev. Lett.* **119** (2017) 181302 [[1708.06917](#)].
- [9] LZ collaboration, J. Aalbers et al., *First Dark Matter Search Results from the LUX-ZEPLIN (LZ) Experiment*, *Phys. Rev. Lett.* **131** (2023) 041002 [[2207.03764](#)].
- [10] PAMELA collaboration, O. Adriani et al., *PAMELA results on the cosmic-ray antiproton flux from 60 MeV to 180 GeV in kinetic energy*, *Phys. Rev. Lett.* **105** (2010) 121101 [[1007.0821](#)].
- [11] FERMI-LAT collaboration, M. Ackermann et al., *Measurement of separate cosmic-ray electron and positron spectra with the Fermi Large Area Telescope*, *Phys. Rev. Lett.* **108** (2012) 011103 [[1109.0521](#)].
- [12] AMS 01 collaboration, M. Aguilar et al., *Cosmic-ray positron fraction measurement from 1 to 30-GeV with AMS-01*, *Phys. Lett. B* **646** (2007) 145 [[astro-ph/0703154](#)].
- [13] J. Goodman, M. Ibe, A. Rajaraman, W. Shepherd, T. M. P. Tait and H.-B. Yu, *Constraints on Light Majorana dark Matter from Colliders*, *Phys. Lett. B* **695** (2011) 185 [[1005.1286](#)].
- [14] P. J. Fox, R. Harnik, J. Kopp and Y. Tsai, *Missing Energy Signatures of Dark Matter at the LHC*, *Phys. Rev. D* **85** (2012) 056011 [[1109.4398](#)].
- [15] J. Cao, L. Meng, Y. Yue, H. Zhou and P. Zhu, *Suppressing the scattering of WIMP dark matter and nucleons in supersymmetric theories*, *Phys. Rev. D* **101** (2020) 075003 [[1910.14317](#)].
- [16] J. F. Gunion and H. E. Haber, *Higgs Bosons in Supersymmetric Models. 1.*, *Nucl. Phys. B* **272** (1986) 1.
- [17] H. E. Haber and G. L. Kane, *The Search for Supersymmetry: Probing Physics Beyond the Standard Model*, *Phys. Rept.* **117** (1985) 75.
- [18] A. Djouadi, *The Anatomy of electro-weak symmetry breaking. II. The Higgs bosons in the minimal supersymmetric model*, *Phys. Rept.* **459** (2008) 1 [[hep-ph/0503173](#)].
- [19] Y. He, L. Meng, Y. Yue and D. Zhang, *Impact of the recent measurement of $(g-2)_\mu$, the LHC search for supersymmetry, and the LZ experiment on the minimal supersymmetric standard model*, *Phys. Rev. D* **108** (2023) 115010 [[2303.02360](#)].
- [20] S. Bisal, A. Chatterjee, D. Das and S. A. Pasha, *Radiative corrections to aid the direct detection of the Higgsino-like neutralino dark matter: Spin-independent interactions*, *Phys. Rev. D* **110** (2024) 023043 [[2311.09937](#)].
- [21] S. Bisal, A. Chatterjee, D. Das and S. A. Pasha, *Confronting electroweak MSSM through one-loop renormalized neutralino-Higgs interactions for dark matter direct detection and the muon $g-2$* , *Phys. Rev. D* **110** (2024) 015021 [[2311.09938](#)].
- [22] G. F. Giudice and A. Masiero, *A Natural Solution to the mu Problem in Supergravity Theories*, *Phys. Lett. B* **206** (1988) 480.

- [23] A. Arvanitaki, M. Baryakhtar, X. Huang, K. van Tilburg and G. Villadoro, *The Last Vestiges of Naturalness*, *JHEP* **03** (2014) 022 [[1309.3568](#)].
- [24] J. A. Evans, Y. Kats, D. Shih and M. J. Strassler, *Toward Full LHC Coverage of Natural Supersymmetry*, *JHEP* **07** (2014) 101 [[1310.5758](#)].
- [25] H. Baer, V. Barger, D. Mickelson and M. Padeffke-Kirkland, *SUSY models under siege: LHC constraints and electroweak fine-tuning*, *Phys. Rev. D* **89** (2014) 115019 [[1404.2277](#)].
- [26] U. Ellwanger, C. Hugonie and A. M. Teixeira, *The Next-to-Minimal Supersymmetric Standard Model*, *Phys. Rept.* **496** (2010) 1 [[0910.1785](#)].
- [27] M. Maniatis, *The Next-to-Minimal Supersymmetric extension of the Standard Model reviewed*, *Int. J. Mod. Phys. A* **25** (2010) 3505 [[0906.0777](#)].
- [28] J. Cao, Y. He, L. Shang, W. Su and Y. Zhang, *Natural NMSSM after LHC Run I and the Higgsino dominated dark matter scenario*, *JHEP* **08** (2016) 037 [[1606.04416](#)].
- [29] U. Ellwanger, *Present Status and Future Tests of the Higgsino-Singlino Sector in the NMSSM*, *JHEP* **02** (2017) 051 [[1612.06574](#)].
- [30] Q.-F. Xiang, X.-J. Bi, P.-F. Yin and Z.-H. Yu, *Searching for Singlino-Higgsino Dark Matter in the NMSSM*, *Phys. Rev. D* **94** (2016) 055031 [[1606.02149](#)].
- [31] J. Cao, Y. He, L. Shang, Y. Zhang and P. Zhu, *Current status of a natural NMSSM in light of LHC 13 TeV data and XENON-1T results*, *Phys. Rev. D* **99** (2019) 075020 [[1810.09143](#)].
- [32] U. Ellwanger and C. Hugonie, *The higgsino–singlino sector of the NMSSM: combined constraints from dark matter and the LHC*, *Eur. Phys. J. C* **78** (2018) 735 [[1806.09478](#)].
- [33] F. Domingo, J. S. Kim, V. M. Lozano, P. Martin-Ramiro and R. Ruiz de Austri, *Confronting the neutralino and chargino sector of the NMSSM with the multilepton searches at the LHC*, *Phys. Rev. D* **101** (2020) 075010 [[1812.05186](#)].
- [34] S. Baum, N. R. Shah and K. Freese, *The NMSSM is within Reach of the LHC: Mass Correlations & Decay Signatures*, *JHEP* **04** (2019) 011 [[1901.02332](#)].
- [35] M. van Beekveld, S. Caron and R. Ruiz de Austri, *The current status of fine-tuning in supersymmetry*, *JHEP* **01** (2020) 147 [[1906.10706](#)].
- [36] W. Abdallah, A. Chatterjee and A. Datta, *Revisiting singlino dark matter of the natural Z_3 -symmetric NMSSM in the light of LHC*, *JHEP* **09** (2019) 095 [[1907.06270](#)].
- [37] M. Guchait and A. Roy, *Light Singlino Dark Matter at the LHC*, *Phys. Rev. D* **102** (2020) 075023 [[2005.05190](#)].
- [38] W. Abdallah, A. Datta and S. Roy, *A relatively light, highly bino-like dark matter*

- in the Z_3 -symmetric NMSSM and recent LHC searches, *JHEP* **04** (2021) 122 [[2012.04026](#)].
- [39] D. Das, U. Ellwanger and A. M. Teixeira, *Modified Signals for Supersymmetry in the NMSSM with a Singlino-like LSP*, *JHEP* **04** (2012) 067 [[1202.5244](#)].
 - [40] U. Ellwanger and A. M. Teixeira, *NMSSM with a singlino LSP: possible challenges for searches for supersymmetry at the LHC*, *JHEP* **10** (2014) 113 [[1406.7221](#)].
 - [41] A. Chatterjee, A. Datta and S. Roy, *Electroweak phase transition in the Z_3 -invariant NMSSM: Implications of LHC and Dark matter searches and prospects of detecting the gravitational waves*, *JHEP* **06** (2022) 108 [[2202.12476](#)].
 - [42] J. Cao, F. Li, J. Lian, Y. Pan and D. Zhang, *Impact of LHC probes of SUSY and recent measurement of $(g - 2)_\mu$ on Z_3 -NMSSM*, *Sci. China Phys. Mech. Astron.* **65** (2022) 291012 [[2204.04710](#)].
 - [43] A. Datta, M. Guchait, A. Roy and S. Roy, *Hunting ewinos and a light scalar of Z_3 -NMSSM with a bino-like dark matter in top squark decays at the LHC*, *JHEP* **11** (2023) 081 [[2211.05905](#)].
 - [44] J. Cao, L. Meng and Y. Yue, *Electron and muon anomalous magnetic moments in the Z_3 -NMSSM*, *Phys. Rev. D* **108** (2023) 035043 [[2306.06854](#)].
 - [45] S. Roy and C. E. M. Wagner, *Dark Matter searches with photons at the LHC*, *JHEP* **04** (2024) 106 [[2401.08917](#)].
 - [46] S. Bisal and D. Das, *Testing Z boson rare decays $Z \rightarrow H_1\gamma, A_1\gamma$ with $(g - 2)_\mu, M_W$, and $BR(h_{SM} \rightarrow Z\gamma)$ in the NMSSM*, *Eur. Phys. J. C* **84** (2024) 630 [[2308.06558](#)].
 - [47] H. Zhou, J. Cao, J. Lian and D. Zhang, *Singlino-dominated dark matter in Z_3 -symmetric NMSSM*, *Phys. Rev. D* **104** (2021) 015017 [[2102.05309](#)].
 - [48] H. Jeffreys, *Theory of probability*, Oxford Classic Texts in the Physical Sciences. The Clarendon Press, Oxford University Press, New York, 1998.
 - [49] J. Cao, D. Li, J. Lian, Y. Yue and H. Zhou, *Singlino-dominated dark matter in general NMSSM*, *JHEP* **06** (2021) 176 [[2102.05317](#)].
 - [50] J. Cao, X. Jia, L. Meng, Y. Yue and D. Zhang, *Status of the singlino-dominated dark matter in general Next-to-Minimal Supersymmetric Standard Model*, *JHEP* **03** (2023) 198 [[2210.08769](#)].
 - [51] M. Pospelov, A. Ritz and M. B. Voloshin, *Secluded WIMP Dark Matter*, *Phys. Lett. B* **662** (2008) 53 [[0711.4866](#)].
 - [52] W. G. Hollik, S. Liebler, G. Moortgat-Pick, S. Paßehr and G. Weiglein, *Phenomenology of the inflation-inspired NMSSM at the electroweak scale*, *Eur. Phys. J. C* **79** (2019) 75 [[1809.07371](#)].
 - [53] W. G. Hollik, G. Weiglein and J. Wittbrodt, *Impact of Vacuum Stability Constraints on the Phenomenology of Supersymmetric Models*, *JHEP* **03** (2019) 109 [[1812.04644](#)].

- [54] U. Ellwanger, *NONRENORMALIZABLE INTERACTIONS FROM SUPERGRAVITY, QUANTUM CORRECTIONS AND EFFECTIVE LOW-ENERGY THEORIES*, *Phys. Lett. B* **133** (1983) 187.
- [55] S. A. Abel, *Destabilizing divergences in the NMSSM*, *Nucl. Phys. B* **480** (1996) 55 [[hep-ph/9609323](#)].
- [56] C. F. Kolda, S. Pokorski and N. Polonsky, *Stabilized singlets in supergravity as a source of the μ - parameter*, *Phys. Rev. Lett.* **80** (1998) 5263 [[hep-ph/9803310](#)].
- [57] C. Panagiotakopoulos and K. Tamvakis, *Stabilized NMSSM without domain walls*, *Phys. Lett. B* **446** (1999) 224 [[hep-ph/9809475](#)].
- [58] G. G. Ross and K. Schmidt-Hoberg, *The Fine-Tuning of the Generalised NMSSM*, *Nucl. Phys. B* **862** (2012) 710 [[1108.1284](#)].
- [59] H. M. Lee, S. Raby, M. Ratz, G. G. Ross, R. Schieren, K. Schmidt-Hoberg et al., *A unique \mathbb{Z}_4^R symmetry for the MSSM*, *Phys. Lett. B* **694** (2011) 491 [[1009.0905](#)].
- [60] H. M. Lee, S. Raby, M. Ratz, G. G. Ross, R. Schieren, K. Schmidt-Hoberg et al., *Discrete R symmetries for the MSSM and its singlet extensions*, *Nucl. Phys. B* **850** (2011) 1 [[1102.3595](#)].
- [61] G. G. Ross, K. Schmidt-Hoberg and F. Staub, *The Generalised NMSSM at One Loop: Fine Tuning and Phenomenology*, *JHEP* **08** (2012) 074 [[1205.1509](#)].
- [62] J.-J. Cao, Z.-X. Heng, J. M. Yang, Y.-M. Zhang and J.-Y. Zhu, *A SM-like Higgs near 125 GeV in low energy SUSY: a comparative study for MSSM and NMSSM*, *JHEP* **03** (2012) 086 [[1202.5821](#)].
- [63] D. J. Miller, R. Nevzorov and P. M. Zerwas, *The Higgs sector of the next-to-minimal supersymmetric standard model*, *Nucl. Phys. B* **681** (2004) 3 [[hep-ph/0304049](#)].
- [64] ATLAS collaboration, G. Aad et al., *Search for heavy Higgs bosons decaying into two tau leptons with the ATLAS detector using pp collisions at $\sqrt{s} = 13$ TeV*, *Phys. Rev. Lett.* **125** (2020) 051801 [[2002.12223](#)].
- [65] ATLAS collaboration, G. Aad et al., *Search for charged Higgs bosons decaying into a top quark and a bottom quark at $\sqrt{s} = 13$ TeV with the ATLAS detector*, *JHEP* **06** (2021) 145 [[2102.10076](#)].
- [66] M. Badziak, M. Olechowski and P. Szczerbiak, *Spin-dependent constraints on blind spots for thermal singlino-higgsino dark matter with(out) light singlets*, *JHEP* **07** (2017) 050 [[1705.00227](#)].
- [67] M. Badziak, M. Olechowski and P. Szczerbiak, *Blind spots for neutralinos in NMSSM with light singlet scalar*, *PoS PLANCK2015* (2015) 130 [[1601.00768](#)].
- [68] C. Cheung, M. Papucci, D. Sanford, N. R. Shah and K. M. Zurek, *NMSSM Interpretation of the Galactic Center Excess*, *Phys. Rev. D* **90** (2014) 075011 [[1406.6372](#)].

- [69] K. Griest and D. Seckel, *Three exceptions in the calculation of relic abundances*, *Phys. Rev. D* **43** (1991) 3191.
- [70] T. Nihei, L. Roszkowski and R. Ruiz de Austri, *Exact cross-sections for the neutralino WIMP pair annihilation*, *JHEP* **03** (2002) 031 [[hep-ph/0202009](#)].
- [71] G. Arcadi, M. Dutra, P. Ghosh, M. Lindner, Y. Mambrini, M. Pierre et al., *The waning of the WIMP? A review of models, searches, and constraints*, *Eur. Phys. J. C* **78** (2018) 203 [[1703.07364](#)].
- [72] M. J. Baker et al., *The Coannihilation Codex*, *JHEP* **12** (2015) 120 [[1510.03434](#)].
- [73] A. Pierce, N. R. Shah and K. Freese, *Neutralino Dark Matter with Light Staus*, [1309.7351](#).
- [74] M. Drees and M. Nojiri, *Neutralino - nucleon scattering revisited*, *Phys. Rev. D* **48** (1993) 3483 [[hep-ph/9307208](#)].
- [75] M. Drees and M. M. Nojiri, *New contributions to coherent neutralino - nucleus scattering*, *Phys. Rev. D* **47** (1993) 4226 [[hep-ph/9210272](#)].
- [76] G. Belanger, F. Boudjema, A. Pukhov and A. Semenov, *Dark matter direct detection rate in a generic model with micrOMEGAs 2.2*, *Comput. Phys. Commun.* **180** (2009) 747 [[0803.2360](#)].
- [77] J. M. Alarcon, J. Martin Camalich and J. A. Oller, *The chiral representation of the πN scattering amplitude and the pion-nucleon sigma term*, *Phys. Rev. D* **85** (2012) 051503 [[1110.3797](#)].
- [78] J. M. Alarcon, L. S. Geng, J. Martin Camalich and J. A. Oller, *The strangeness content of the nucleon from effective field theory and phenomenology*, *Phys. Lett. B* **730** (2014) 342 [[1209.2870](#)].
- [79] ATLAS collaboration, G. Aad et al., *Interpretations of the ATLAS measurements of Higgs boson production and decay rates and differential cross-sections in pp collisions at $\sqrt{s} = 13$ TeV*, [2402.05742](#).
- [80] P. Huang and C. E. M. Wagner, *Blind Spots for neutralino Dark Matter in the MSSM with an intermediate m_A* , *Phys. Rev. D* **90** (2014) 015018 [[1404.0392](#)].
- [81] M. Badziak, M. Olechowski and P. Szczerbiak, *Blind spots for neutralino dark matter in the NMSSM*, *JHEP* **03** (2016) 179 [[1512.02472](#)].
- [82] F. Staub, *SARAH*, [0806.0538](#).
- [83] F. Staub, *SARAH 3.2: Dirac Gauginos, UFO output, and more*, *Comput. Phys. Commun.* **184** (2013) 1792 [[1207.0906](#)].
- [84] F. Staub, *SARAH 4 : A tool for (not only SUSY) model builders*, *Comput. Phys. Commun.* **185** (2014) 1773 [[1309.7223](#)].
- [85] F. Staub, *Exploring new models in all detail with SARAH*, *Adv. High Energy Phys.* **2015** (2015) 840780 [[1503.04200](#)].

- [86] W. Porod, *SPheno, a program for calculating supersymmetric spectra, SUSY particle decays and SUSY particle production at e^+e^- colliders*, *Comput. Phys. Commun.* **153** (2003) 275 [[hep-ph/0301101](#)].
- [87] W. Porod and F. Staub, *SPheno 3.1: Extensions including flavour, CP-phases and models beyond the MSSM*, *Comput. Phys. Commun.* **183** (2012) 2458 [[1104.1573](#)].
- [88] W. Porod, F. Staub and A. Vicente, *A Flavor Kit for BSM models*, *Eur. Phys. J. C* **74** (2014) 2992 [[1405.1434](#)].
- [89] G. Belanger, F. Boudjema, A. Pukhov and A. Semenov, *MicrOMEGAs: A Program for calculating the relic density in the MSSM*, *Comput. Phys. Commun.* **149** (2002) 103 [[hep-ph/0112278](#)].
- [90] G. Belanger, F. Boudjema, C. Hugonie, A. Pukhov and A. Semenov, *Relic density of dark matter in the NMSSM*, *JCAP* **09** (2005) 001 [[hep-ph/0505142](#)].
- [91] G. Belanger, F. Boudjema, A. Pukhov and A. Semenov, *MicrOMEGAs 2.0: A Program to calculate the relic density of dark matter in a generic model*, *Comput. Phys. Commun.* **176** (2007) 367 [[hep-ph/0607059](#)].
- [92] G. Belanger, F. Boudjema, A. Pukhov and A. Semenov, *micrOMEGAs: A Tool for dark matter studies*, *Nuovo Cim. C* **033N2** (2010) 111 [[1005.4133](#)].
- [93] G. Belanger, F. Boudjema, A. Pukhov and A. Semenov, *micrOMEGAs-3: A program for calculating dark matter observables*, *Comput. Phys. Commun.* **185** (2014) 960 [[1305.0237](#)].
- [94] D. Barducci, G. Belanger, J. Bernon, F. Boudjema, J. Da Silva, S. Kraml et al., *Collider limits on new physics within micrOMEGAs-4.3*, *Comput. Phys. Commun.* **222** (2018) 327 [[1606.03834](#)].
- [95] A. Fowlie and M. H. Bardsley, *Superplot: a graphical interface for plotting and analysing MultiNest output*, *Eur. Phys. J. Plus* **131** (2016) 391 [[1603.00555](#)].
- [96] S. Matsumoto, S. Mukhopadhyay and Y.-L. S. Tsai, *Effective Theory of WIMP Dark Matter supplemented by Simplified Models: Singlet-like Majorana fermion case*, *Phys. Rev. D* **94** (2016) 065034 [[1604.02230](#)].
- [97] P. Bechtle, S. Heinemeyer, O. Stål, T. Stefaniak and G. Weiglein, *HiggsSignals: Confronting arbitrary Higgs sectors with measurements at the Tevatron and the LHC*, *Eur. Phys. J. C* **74** (2014) 2711 [[1305.1933](#)].
- [98] O. Stål and T. Stefaniak, *Constraining extended Higgs sectors with HiggsSignals*, *PoS EPS-HEP2013* (2013) 314 [[1310.4039](#)].
- [99] P. Bechtle, S. Heinemeyer, O. Stål, T. Stefaniak and G. Weiglein, *Probing the Standard Model with Higgs signal rates from the Tevatron, the LHC and a future ILC*, *JHEP* **11** (2014) 039 [[1403.1582](#)].
- [100] P. Bechtle, S. Heinemeyer, T. Klingl, T. Stefaniak, G. Weiglein and J. Wittbrodt, *HiggsSignals-2: Probing new physics with precision Higgs measurements in the LHC 13 TeV era*, *Eur. Phys. J. C* **81** (2021) 145 [[2012.09197](#)].

- [101] P. Bechtle, O. Brein, S. Heinemeyer, G. Weiglein and K. E. Williams, *HiggsBounds: Confronting Arbitrary Higgs Sectors with Exclusion Bounds from LEP and the Tevatron*, *Comput. Phys. Commun.* **181** (2010) 138 [[0811.4169](#)].
- [102] P. Bechtle, O. Brein, S. Heinemeyer, G. Weiglein and K. E. Williams, *HiggsBounds 2.0.0: Confronting Neutral and Charged Higgs Sector Predictions with Exclusion Bounds from LEP and the Tevatron*, *Comput. Phys. Commun.* **182** (2011) 2605 [[1102.1898](#)].
- [103] P. Bechtle, O. Brein, S. Heinemeyer, O. Stal, T. Stefaniak, G. Weiglein et al., *Recent Developments in HiggsBounds and a Preview of HiggsSignals*, *PoS CHARGED2012* (2012) 024 [[1301.2345](#)].
- [104] P. Bechtle, O. Brein, S. Heinemeyer, O. Stål, T. Stefaniak, G. Weiglein et al., *HiggsBounds – 4: Improved Tests of Extended Higgs Sectors against Exclusion Bounds from LEP, the Tevatron and the LHC*, *Eur. Phys. J. C* **74** (2014) 2693 [[1311.0055](#)].
- [105] P. Bechtle, D. Dercks, S. Heinemeyer, T. Klingl, T. Stefaniak, G. Weiglein et al., *HiggsBounds-5: Testing Higgs Sectors in the LHC 13 TeV Era*, *Eur. Phys. J. C* **80** (2020) 1211 [[2006.06007](#)].
- [106] L. M. Carpenter, R. Colburn, J. Goodman and T. Linden, *Indirect Detection Constraints on s and t Channel Simplified Models of Dark Matter*, *Phys. Rev. D* **94** (2016) 055027 [[1606.04138](#)].
- [107] X.-J. Huang, C.-C. Wei, Y.-L. Wu, W.-H. Zhang and Y.-F. Zhou, *Antiprotons from dark matter annihilation through light mediators and a possible excess in AMS-02 \bar{p}/p data*, *Phys. Rev. D* **95** (2017) 063021 [[1611.01983](#)].
- [108] PARTICLE DATA GROUP collaboration, M. Tanabashi et al., *Review of Particle Physics*, *Phys. Rev. D* **98** (2018) 030001.
- [109] B. O’Leary and J. E. Camargo-Molina, “VevaciousPlusPlus.” <https://github.com/JoseEliei/VevaciousPlusPlus>, 2014.
- [110] J. E. Camargo-Molina, B. O’Leary, W. Porod and F. Staub, *Vevacious: A Tool For Finding The Global Minima Of One-Loop Effective Potentials With Many Scalars*, *Eur. Phys. J. C* **73** (2013) 2588 [[1307.1477](#)].
- [111] CMS collaboration, A. M. Sirunyan et al., *Searches for pair production of charginos and top squarks in final states with two oppositely charged leptons in proton-proton collisions at $\sqrt{s} = 13$ TeV*, *JHEP* **11** (2018) 079 [[1807.07799](#)].
- [112] CMS collaboration, A. M. Sirunyan et al., *Search for supersymmetric partners of electrons and muons in proton-proton collisions at $\sqrt{s} = 13$ TeV*, *Phys. Lett. B* **790** (2019) 140 [[1806.05264](#)].
- [113] CMS collaboration, A. M. Sirunyan et al., *Combined search for electroweak production of charginos and neutralinos in proton-proton collisions at $\sqrt{s} = 13$ TeV*, *JHEP* **03** (2018) 160 [[1801.03957](#)].

- [114] CMS collaboration, A. M. Sirunyan et al., *Search for supersymmetry with Higgs boson to diphoton decays using the razor variables at $\sqrt{s} = 13$ TeV*, *Phys. Lett. B* **779** (2018) 166 [[1709.00384](#)].
- [115] CMS collaboration, A. M. Sirunyan et al., *Search for electroweak production of charginos and neutralinos in multilepton final states in proton-proton collisions at $\sqrt{s} = 13$ TeV*, *JHEP* **03** (2018) 166 [[1709.05406](#)].
- [116] CMS collaboration, A. M. Sirunyan et al., *Search for new phenomena in final states with two opposite-charge, same-flavor leptons, jets, and missing transverse momentum in pp collisions at $\sqrt{s} = 13$ TeV*, *JHEP* **03** (2018) 076 [[1709.08908](#)].
- [117] ATLAS collaboration, M. Aaboud et al., *Search for electroweak production of supersymmetric particles in final states with two or three leptons at $\sqrt{s} = 13$ TeV with the ATLAS detector*, *Eur. Phys. J. C* **78** (2018) 995 [[1803.02762](#)].
- [118] ATLAS collaboration, M. Aaboud et al., *Search for chargino and neutralino production in final states with a Higgs boson and missing transverse momentum at $\sqrt{s} = 13$ TeV with the ATLAS detector*, *Phys. Rev. D* **100** (2019) 012006 [[1812.09432](#)].
- [119] ATLAS collaboration, M. Aaboud et al., *Search for chargino-neutralino production using recursive jigsaw reconstruction in final states with two or three charged leptons in proton-proton collisions at $\sqrt{s} = 13$ TeV with the ATLAS detector*, *Phys. Rev. D* **98** (2018) 092012 [[1806.02293](#)].
- [120] ATLAS collaboration, G. Aad et al., *Search for chargino-neutralino production with mass splittings near the electroweak scale in three-lepton final states in $\sqrt{s} = 13$ TeV pp collisions with the ATLAS detector*, *Phys. Rev. D* **101** (2020) 072001 [[1912.08479](#)].
- [121] ATLAS collaboration, G. Aad et al., *Search for electroweak production of charginos and sleptons decaying into final states with two leptons and missing transverse momentum in $\sqrt{s} = 13$ TeV pp collisions using the ATLAS detector*, *Eur. Phys. J. C* **80** (2020) 123 [[1908.08215](#)].
- [122] ATLAS collaboration, G. Aad et al., *Search for direct production of electroweakinos in final states with one lepton, missing transverse momentum and a Higgs boson decaying into two b-jets in pp collisions at $\sqrt{s} = 13$ TeV with the ATLAS detector*, *Eur. Phys. J. C* **80** (2020) 691 [[1909.09226](#)].
- [123] CMS collaboration, A. M. Sirunyan et al., *Search for supersymmetry in final states with two oppositely charged same-flavor leptons and missing transverse momentum in proton-proton collisions at $\sqrt{s} = 13$ TeV*, *JHEP* **04** (2021) 123 [[2012.08600](#)].
- [124] ATLAS collaboration, G. Aad et al., *Search for chargino-neutralino pair production in final states with three leptons and missing transverse momentum in $\sqrt{s} = 13$ TeV pp collisions with the ATLAS detector*, *Eur. Phys. J. C* **81** (2021) 1118 [[2106.01676](#)].

- [125] ATLAS collaboration, G. Aad et al., *Search for direct production of electroweakinos in final states with one lepton, missing transverse momentum and a Higgs boson decaying into two b-jets in pp collisions at $\sqrt{s} = 13$ TeV with the ATLAS detector*, *Eur. Phys. J. C* **80** (2020) 691 [[1909.09226](#)].
- [126] ATLAS collaboration, G. Aad et al., *Search for charginos and neutralinos in final states with two boosted hadronically decaying bosons and missing transverse momentum in pp collisions at $\sqrt{s} = 13$ TeV with the ATLAS detector*, *Phys. Rev. D* **104** (2021) 112010 [[2108.07586](#)].
- [127] ATLAS collaboration, M. Aaboud et al., *Search for photonic signatures of gauge-mediated supersymmetry in 13 TeV pp collisions with the ATLAS detector*, *Phys. Rev. D* **97** (2018) 092006 [[1802.03158](#)].
- [128] ATLAS collaboration, G. Aad et al., *Search for supersymmetry in events with four or more charged leptons in 139 fb^{-1} of $\sqrt{s} = 13$ TeV pp collisions with the ATLAS detector*, *JHEP* **07** (2021) 167 [[2103.11684](#)].
- [129] ATLAS collaboration, G. Aad et al., *Searches for electroweak production of supersymmetric particles with compressed mass spectra in $\sqrt{s} = 13$ TeV pp collisions with the ATLAS detector*, *Phys. Rev. D* **101** (2020) 052005 [[1911.12606](#)].
- [130] ATLAS collaboration, M. Aaboud et al., *Search for electroweak production of supersymmetric states in scenarios with compressed mass spectra at $\sqrt{s} = 13$ TeV with the ATLAS detector*, *Phys. Rev. D* **97** (2018) 052010 [[1712.08119](#)].
- [131] CMS collaboration, A. M. Sirunyan et al., *Search for new physics in events with two soft oppositely charged leptons and missing transverse momentum in proton-proton collisions at $\sqrt{s} = 13$ TeV*, *Phys. Lett. B* **782** (2018) 440 [[1801.01846](#)].
- [132] F. Feroz, M. P. Hobson and M. Bridges, *MultiNest: an efficient and robust Bayesian inference tool for cosmology and particle physics*, *Mon. Not. Roy. Astron. Soc.* **398** (2009) 1601 [[0809.3437](#)].
- [133] F. Feroz, M. P. Hobson, E. Cameron and A. N. Pettitt, *Importance Nested Sampling and the MultiNest Algorithm*, *Open J. Astrophys.* **2** (2019) 10 [[1306.2144](#)].
- [134] C. K. Khosa, S. Kraml, A. Lessa, P. Neuhuber and W. Waltenberger, *SModelS Database Update v1.2.3*, *LHEP* **2020** (2020) 158 [[2005.00555](#)].
- [135] W. Beenakker, R. Hopker and M. Spira, *PROSPINO: A Program for the production of supersymmetric particles in next-to-leading order QCD*, [hep-ph/9611232](#).
- [136] J. Alwall, M. Herquet, F. Maltoni, O. Mattelaer and T. Stelzer, *MadGraph 5 : Going Beyond*, *JHEP* **06** (2011) 128 [[1106.0522](#)].
- [137] E. Conte, B. Fuks and G. Serret, *MadAnalysis 5, A User-Friendly Framework for Collider Phenomenology*, *Comput. Phys. Commun.* **184** (2013) 222 [[1206.1599](#)].

- [138] T. Sjöstrand, S. Ask, J. R. Christiansen, R. Corke, N. Desai, P. Ilten et al., *An introduction to PYTHIA 8.2*, *Comput. Phys. Commun.* **191** (2015) 159 [[1410.3012](#)].
- [139] DELPHES 3 collaboration, J. de Favereau, C. Delaere, P. Demin, A. Giammanco, V. Lemaître, A. Mertens et al., *DELPHES 3, A modular framework for fast simulation of a generic collider experiment*, *JHEP* **02** (2014) 057 [[1307.6346](#)].
- [140] M. Drees, H. Dreiner, D. Schmeier, J. Tattersall and J. S. Kim, *CheckMATE: Confronting your Favourite New Physics Model with LHC Data*, *Comput. Phys. Commun.* **187** (2015) 227 [[1312.2591](#)].
- [141] D. Dercks, N. Desai, J. S. Kim, K. Rolbiecki, J. Tattersall and T. Weber, *CheckMATE 2: From the model to the limit*, *Comput. Phys. Commun.* **221** (2017) 383 [[1611.09856](#)].
- [142] J. S. Kim, D. Schmeier, J. Tattersall and K. Rolbiecki, *A framework to create customised LHC analyses within CheckMATE*, *Comput. Phys. Commun.* **196** (2015) 535 [[1503.01123](#)].
- [143] J. Cao, J. Lian, Y. Pan, D. Zhang and P. Zhu, *Improved $(g - 2)_\mu$ measurement and singlino dark matter in μ -term extended \mathbb{Z}_3 -NMSSM*, *JHEP* **09** (2021) 175 [[2104.03284](#)].
- [144] A. Berlin, P. Gratia, D. Hooper and S. D. McDermott, *Hidden Sector Dark Matter Models for the Galactic Center Gamma-Ray Excess*, *Phys. Rev. D* **90** (2014) 015032 [[1405.5204](#)].
- [145] T. Gherghetta, B. von Harling, A. D. Medina, M. A. Schmidt and T. Trott, *SUSY implications from WIMP annihilation into scalars at the Galactic Center*, *Phys. Rev. D* **91** (2015) 105004 [[1502.07173](#)].